



Contents lists available at ScienceDirect

Atmospheric Environment

journal homepage: www.elsevier.com/locate/atmosenv

Real-time quantification and source apportionment of fine particulate matter including organics and elements in Delhi during summertime

Ashutosh K. Shukla^a, Vipul Lalchandani^a, Deepika Bhattu^b, Jay S. Dave^c, Pragati Rai^d, Navaneeth M. Thamban^a, Suneeti Mishra^a, Sreenivas Gaddamidi^a, Nidhi Tripathi^e, Pawan Vats^f, Neeraj Rastogi^c, Lokesh Sahu^e, Dilip Ganguly^f, Mayank Kumar^g, Vikram Singh^h, Prashant Gargavaⁱ, Sachchida N. Tripathi^{a,*}

^a Department of Civil Engineering, Indian Institute of Technology Kanpur, Uttar Pradesh, 208016, India

^b Department of Civil and Infrastructure Engineering, Indian Institute of Technology Jodhpur, Rajasthan, 342037, India

^c Geosciences Division, Physical Research Laboratory, Ahmedabad, 380009, India

^d Laboratory of Atmospheric Chemistry, Paul Scherrer Institute, Villigen, PSI, 5232, Switzerland

^e Space and Atmospheric Sciences Division, Physical Research Laboratory, Ahmedabad, 380009, India

^f Centre for Atmospheric Sciences, Indian Institute of Technology Delhi, New Delhi, 110016, India

^g Department of Mechanical Engineering, Indian Institute of Technology Delhi, New Delhi, 110016, India

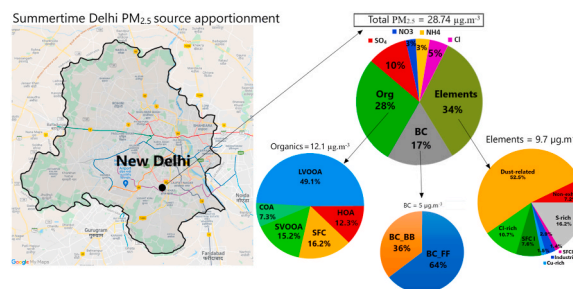
^h Department of Chemical Engineering, Indian Institute of Technology Delhi, New Delhi, 110016, India

ⁱ Central Pollution Control Board, Parivesh Bhawan, East Arjun Nagar, Delhi, 110032, India

HIGHLIGHTS

- First time complete characterization of PM_{2.5} (non-refractory, refractory and elements) during summer in Delhi.
- Source apportionment of highly time-resolved organics and elements from real time instruments.
- Distinct sources are resolved in Delhi during summer along with their potential regions of origin.
- Dust storms and Cl episodes have been captured using high time-resolution AMS and Xact data.
- Secondary oxidized sources dominate the summertime than primary (anthropogenic) sources.

GRAPHICAL ABSTRACT



ARTICLE INFO

Keywords:

Summertime
Source apportionment
Delhi
PM_{2.5}
Organic
Elements and BC

ABSTRACT

Delhi is one of the most polluted cities globally, with frequent severe air pollution episodes and haze events occurring in recent years, thereby compelling us to understand the sources to develop effective mitigation plans. Complete chemical characterization of fine particulate matter (PM_{2.5}) components (non-refractory, refractory and elements) with high time resolution has been done during the summer season (June–July 2019). The total PM equivalent (PM_{2.5(eq)}) was $28.7 \pm 13.2 \mu\text{g m}^{-3}$ of which elements dominated the PM_{2.5(eq)} with 34% contribution followed by organics (28%), black carbon (BC) (17%), SO₄²⁻ (10%), Cl⁻ (5%), NH₄⁺ (3.5%) and NO₃⁻ (2.5%). The contributions from organic aerosols (OA) and SO₄²⁻ were observed to be more than Cl⁻ and NO₃⁻. The total elemental mass concentration (PM_{El}) was mostly contributed (~96%) by Si, S, Cl, Ca, K, Fe and Al with Si

* Corresponding author.

E-mail address: snt@iitk.ac.in (S.N. Tripathi).

<https://doi.org/10.1016/j.atmosenv.2021.118598>

Received 22 November 2020; Received in revised form 25 June 2021; Accepted 30 June 2021

Available online 5 July 2021

1352-2310/© 2021 Elsevier Ltd. All rights reserved.

and S alone contributing around 50% of PM_{EQ} . Crustal elements (Al, Fe, Ca and Si) were highly enhanced in summer than elements emitted from anthropogenic emissions (Cl, S, K, Pb and Zn). Source apportionment (SA) of PM was performed using positive matrix factorization (PMF) together with ME-2 (multilineal engine) for OA and elements, separately. PMF on both datasets helped resolve sources such as combustion, industrial, dust-related, incineration and traffic. OA PMF identified three factors related to primary emissions: hydrocarbon-like OA (HOA, 12.3%), solid fuel combustion (SFC, 16.2%) and cooking OA (COA, 7.3%) and two oxygenated OA (OOA): semi-volatile OOA (SVOOA, 15.2%) and low-volatile OOA (LVOOA, 49.1%). The elemental PMF resolved 8 factors: dust (52.5%), S-rich (16.2%), Cl-rich (10.7%), 2 SFC factors (10.5%), non-exhaust (7.2%), Cu-rich (1.5%) and industrial (1.4%). The contribution of BC to total PM mass is shown to increase in the summer compared to previous studies reported for the winter season. The secondary oxidized sources dominated both the OA and elements SA during the summer with 64.3% and 27% (dust not considered) contribution, respectively. The domination of secondary sources implies that it is crucial to control the secondary aerosols' precursors in Delhi for developing pollution control strategies. The ME-2 resolved factors, coupled with concentration weighted trajectory (CWT) showed the probable major elemental source regions of local origin (Delhi- National Capital Region (Delhi-NCR)) as well as regional (from Punjab, Haryana, Uttar Pradesh and Pakistan). The local sources included Cu-rich (Haryana) and SFC-II (Delhi and Uttar Pradesh), while the regional sources were dust (south-west (SW)), industrial, Cl-rich (north-west (NW)), SFC-I (east and south-east (SE)) and S-rich (SE).

1. Introduction

Atmospheric aerosols have significant effects on human health, visibility, climate forcing and deposition of acids and nutrients to the ecosystem and crops (Molina et al., 2015; Ulbrich et al., 2009). Climate effects include a change in the earth-atmosphere energy budget, atmospheric warming, clouds, and precipitation pattern (IPCC, 2013). Long-term exposure to fine mode aerosols ($PM_{2.5}$) can further cause serious human health effects like cardiovascular and respiratory problems (Pope and Dockery, 2006).

The chemical composition of $PM_{2.5}$, especially metals (Fe, Cu, Mn, Ni, V, Cr, As and Pb) with black carbon (BC), has a prominent role in the severity of the associated toxic effects (Suvvarapu and Baek, 2016). The composition of $PM_{2.5}$ depends on sources, atmospheric reactions, and meteorological conditions. The analysis of PM sources is crucial for reducing emissions and developing pollution control measures (Huang et al., 2015). The high-time resolution source apportionment (SA) study is significant for understanding the dynamics of sources by capturing the diurnal variations of major source activities and secondary formation sources (Li et al., 2020). It also helps to understand the episodic events (Rai et al., 2020b; Rai et al., 2020a) and design effective mitigation strategies.

Receptor models are widely used in SA studies to predict the sources better than other models (Hopke, 2016; Zhang et al., 2011). Several studies have been done using the high-resolution time-of-flight aerosol mass spectrometer (HR-ToF-AMS) data. HR-ToF-AMS provides high-time resolution non-refractory particulate matter (PM), which can be effectively used for positive matrix factorization (PMF). PMF results in a number of constant source profiles and their varying contribution over time (Lanz et al., 2007; Mohr et al., 2012; Sun et al., 2016; Ulbrich et al., 2009). The organic aerosol (OA) sources identified and reported in the previous studies can be broadly classified into primary organic aerosols (POA) and secondary organic aerosols (SOA). POA can be further separated into hydrocarbon-like OA (HOA) which includes traffic; biomass burning organic aerosols (BBOA) may be emitted from crop residue burning, open fire activities, coal and wood burning; cooking OA (COA) from cooking and coal combustion organic aerosols (CCOA) from coal combustion. SOA can be formed from the oxidation of POA or volatile organic compounds (VOCs) in the atmosphere. Several studies have also reported different OOA factors, indicating the advantage of PMF in extracting a low concentration, but distinct factors LVOOA (more oxidized and aged) and SVOOA (less oxidized) (Duan et al., 2019; Mohr et al., 2012; Wang et al., 2017).

Elements are generally a minor contributor to the atmospheric aerosol mass, but they act as specific markers for several emission sources (Rai et al., 2020b). Likewise, high temporal resolution elemental data can provide greater insight into understanding the primary local

sources with considerable temporal variation and episodic events in urban areas. Few such studies, using highly time-resolved elements data have been performed recently in Canada, China and Delhi (Chang et al., 2018; Jeong et al., 2016; Rai et al., 2020b; Rai et al., 2020a). These studies identified distinct sources such as industrial, road dust, crustal dust, secondary chloride, brake and tyre wear, coal-based thermal power plant, biomass burning, traffic, and fireworks events.

Delhi is the most polluted city globally, with an annual mean $PM_{2.5}$ concentration of $98.6 \mu g m^{-3}$ (IQAir report, 2019). Most of the chemical characterization and SA studies (both for organic and elements) in Delhi have been done with the offline filter-based analysis with low time resolution (Jain et al., 2018; Jaiprakash, 2017; Khare and Baruah, 2010; Nagar et al., 2017; Pant et al., 2015; Sharma et al., 2016). The offline analysis provides a good preliminary idea but suffers from some serious drawbacks such as positive and negative artifacts, and not being able to capture the rapid evolution of particles due to its low time resolution. Recently, few SA studies (Bhandari et al., 2020; Lalchandani et al., 2021; Manchanda et al., 2021; Rai et al., 2020b; Tobler et al., 2020) have been conducted in Delhi using real-time high-resolution measurements. Tobler et al. (2020) found HOA, solid fuel combustion OA (SFCOA) and OOA as major factors in their studies while Lalchandani et al. (2021) resolved six factors; HOA, two SFC's and three OOA factors. In addition to the Organics SA study, elemental SA has been done by Rai et al. (2020b) in which nine factors were identified including dust, non-exhaust, two SFC factors, S-rich and four factors related to anthropogenic industrial/combustion plume events.

These are high time resolutions detailed studies which have been reported are mainly focused on the winter season. Although Bhandari et al. (2020) and Tobler et al. (2020) have attempted to identify the sources for multiple seasons, including summer, those don't give a complete picture as they performed only on the part of PM (only organics) using Aerosol Chemical Speciation Monitor (ACSM). No such study has yet been conducted on metals' high time resolution data in Delhi's summer season. Since most of the studies performed in summer utilize just a part of PM (organics), it is crucial to investigate the complete speciation of PM (organics, metals and BC) and their sources to understand the inhomogeneity in the seasonal contribution to pollution.

Duan et al. (2019) discussed the inhomogeneity in the contribution to PM pollution depending on different sampling seasons, highlighting the need for more studies on chemical composition, sources and atmospheric evolution of PM. Hu et al. (2016) reported a stable ~80% contribution of secondary species to PM_1 in summertime Beijing, while PM_1 mass concentration in winter changed dramatically due to different meteorological conditions and enhanced primary emissions. This work focuses on providing a complete characterization of $PM_{2.5}$ (non-refractory- $PM_{2.5}$ (NR- $PM_{2.5}$)) (organic and inorganic), elements and BC) as well as a comprehensive picture of the sources of $PM_{2.5}$ by real-time

SA study (for both organics and elements in separate PMF analysis) for the first-time during summer (June–July 2019) in Delhi. It also helps in understanding the seasonal contribution of sources and their characteristics by comparing the results with the previous studies performed at the same site during the winter season.

2. Material and methods

2.1. Sampling site

The Delhi National Capital Territory (NCT) covers a 1483 km² area and has a dense population of over 19 million people, with a total vehicle population of 10.9 million (Economic Survey of Delhi, 2018–19). The NCT of Delhi has a semi-arid climate, with dust storms from the Sahara, Arabian deserts, Gulf and Thar deserts primarily influencing the summer season (Beig et al., 2019). High temperature variability is observed between winter (~2 °C–15 °C) and summer (~35 °C–48 °C) along with high diel variations. The average temperature, relative humidity (RH), and wind speed for the sampling period were 33 ± 4 °C, 58 ± 20%, and 5.4 ± 4.9 km h⁻¹, respectively (Fig. S2).

The instruments (as mentioned in the subsequent section) were deployed on the third floor (12m above ground) block VI of the Centre for Atmospheric Science (CAS) laboratory building of the Indian Institute of Technology Delhi (IITD) campus (28.54°N, 77.19°E) (Rai et al., 2020b; Wang et al., 2020). The measurements of NR-PM_{2.5} (organic and inorganic), elements and BC were conducted during summer precisely from May 31, 2019 to July 26, 2019. The IITD campus is in south Delhi and is surrounded by various residential and commercial buildings and a major road ~150 m away from the sampling location.

2.2. Sampling details and instrumentation

A suite of semi-online and online instruments was installed at the IITD site to investigate PM_{2.5} components, their chemical properties, evolution, and sources. The instruments included HR-ToF-AMS (Aerodyne Research Inc., Billerica, MA, USA) (DeCarlo et al., 2006) for NR-PM_{2.5}, Xact 625i ambient metal monitor (Cooper Environmental Services, Beaverton, Oregon, USA) (Rai et al., 2020a) for elements, and a seven wavelength aethalometer mode AE-33 (Aerosol d.o.o, Ljubljana, Slovenia) (Drinovec et al., 2015) for BC measurements.

Ambient aerosols were sampled continuously at a flow rate of 5.0 L per min (lpm) through a PM_{2.5} cyclone (BGI, Mesa Labs. Inc) inlet with stainless steel tubing installed on the rooftop. The steel tubing was connected parallel to a Nafion Dryer (MD-110-144P-4; Perma Pure, Halma, UK) and the combined NO_x (ECOTECH Model: Serinus 40 Oxides of Nitrogen Analyzer) and CO (ECOTECH Serinus 30 CO Analyzer) analyzer (flow rate of 1.61 lpm). Then the Nafion dryer output flow was split between AMS (0.08 lpm) and combined instruments which included an Aethalometer (3.0 lpm) and SMPS (0.3 lpm). The sampling line for the Xact metal monitor was separate and a heater was set up at the end of the long sampling tube. The heater power was adjusted to ensure the 45% RH set point (Xact instrument has temperature and RH sensors) and avoid water deposition at Teflon tape.

2.2.1. High-resolution time-of-flight aerosol mass spectrometer (HR-ToF-AMS)

HR-ToF AMS measures size-resolved mass concentration and chemical composition of NR fraction of PM_{2.5} (depending on the aerodynamic lens) with a time resolution of 2 min. The NR aerosols are defined as particles that are flash vaporized at high temperatures (600 °C) and include organics, nitrate (NO₃⁻), sulfate (SO₄²⁻), ammonium (NH₄⁺) and chloride (Cl⁻). A detailed description of the instrument's working has been provided in the literature by DeCarlo et al. (2006). In summary, the ambient aerosol is sampled through a critical orifice of 100 μm and focused by an aerodynamic lens further into the sizing chamber. The focused beam then reaches the high vacuum particle sizing chamber

with a mechanical chopper that alternates between fully open, fully closed and chopped positions. The size segregated particles now move towards the vaporizer (600 °C) and get flash vaporized. The vaporized molecules are ionized using an electron ionizer (70 eV) and finally ions are detected by the mass spectrometer. The instrument was operated only in V-mode (higher sensitivity and lower resolving power) and during the 2 min sampling time four cycles of 30 s alternate for each in the mass spectrum (MS) and particle time-of-flight (P-ToF) mode alternatively.

The raw AMS data was analyzed using SQUIRREL v1.61 (for UMR analysis) and PIKA V1.23 (for HR analysis) in Igor Pro 6.37 (WaveMetrics, Portland, USA). The CDCE was calculated according to the method of Middlebrook et al. (2012). A collection efficiency (CE) value of one was assumed for the AMS capture vaporizer (Hu et al., 2017). Ionization efficiency (IE) calibrations were performed at the start and in the middle of the campaign using a monodisperse particle of diameter 300 nm of ammonium nitrate and ammonium sulfate using a scanning mobility particle analyzer (SMPS) (Grimm model). The Relative IE (RIE) of ammonium at the start and middle of the campaign were 4.68 and 4.78, respectively and that of sulfate was 1.67, which was calculated based on the IE calibrations using ammonium nitrate and ammonium sulfate while a standard RIE with a value of 1.4 and 1.3 was used for Organics and Chloride, respectively.

2.2.2. Xact 625i ambient metal monitor

The Xact ambient metal monitor is designed to measure online, near real-time concentration of elements in aerosols. A detailed description of the instrument and its working principle is provided in the literature (Battele, 2012). Briefly, the ambient aerosol is sampled at the flow rate of 16.7 lpm. The sampled aerosol deposits on the filter tape (deposit area 0.487 cm²) advanced to the analysis area using energy dispersive X-ray fluorescence (EDXRF). In this technique, the X-ray irradiates the deposited area using three energy conditions (EC). The excited X-ray fluorescence (XRF) is measured by a silicon drift detector (SDD). After that, using spectral deconvolution technique, it is found that which element contributed to the spectral peak intensity and then finally using an analysis software the elemental concentrations are obtained.

The Xact metal monitor was set up on a half-hourly time resolution to measure the following 30 elements: Al, Si, S, Cl, K, Ca, Ti, Cr, Mn, Fe, Co, Ni, Cu, Zn, As, Se, Br, Rb, Sr, Zr, Mo, Cd, In, Sn, Sb, Te, Ba, Pb, and Bi. The quality assurance/quality control (QA/QC) of the instrument setup was ensured by calibrating the flow rate using a standard flowmeter (Field flow calibrator, ALICAT scientific) and regulated via ambient temperature and pressure measurements. The internal energy alignments and intensity checks of a known sample for Chromium (Cr), Lead (Pb) and Cadmium (Cd) were automatically conducted every midnight (00:15 to 00:30). The energy alignment process uses a Cr and Niobium (Nb) rod to ensure that the spectral peaks for each element are at the correct energy levels. Daily QA Upscale data for these metals were within ±10%.

Further to check for the instrument's stability, an internal Nb source is measured with each ambient sample. The XRF calibration was done using the thin film standards of elements and the result was well within the limit of ±5% and the leak check and flow check was done at the beginning and end of the campaign during summer. The cyclone was cleaned at regular intervals due to high loadings from the dust storms.

2.2.3. Black carbon (BC) and supporting measurements

The real-time BC concentration was measured by the Aethalometer (AE-33, Magee Scientific, Berkeley, CA, USA). It measures the light attenuation using dual spot technology (to correct the nonlinearity of both the filter loading effects and aerosol loads with different flow rates) at seven different wavelengths (370, 470, 520, 590, 660, 880 and 950 nm) with 1-min time resolution. The light absorption measurement at 880 nm was converted to BC concentration using a mass absorption cross-section (MAC) of 7.77 m².g⁻¹ (Drinovec et al., 2015).

Supplementary data was used here only to compare with factors from SA in our study and the data of Proton Transfer Reaction Time-of-Flight Mass Spectrometer (PTR-ToF-MS) is the scope of other studies. Real-time NO_x and CO measurements were performed using gas analyzers for NO_x (ECOTECH Model: Serinus 40 Oxides of Nitrogen Analyzer) and CO (ECOTECH Serinus 30 CO Analyzer). The NO_x analyzer measures the oxides of nitrogen using the gas phase chemiluminescence method, while the CO analyzer measures the carbon monoxide using the Infrared absorption technique (Sahu et al., 2020). PTR-ToF-MS (Ionicon Analytical G.m.b.H., Austria) was used to quantify VOCs, whereas EBAM (MetOne Inc) was used to assess PM2.5 mass concentration.

2.3. Source apportionment (SA) using ME-2

PMF is a bilinear unmixing receptor model with non-negative constraints and is widely used for the SA of ambient measurements (Paatero and Tapper, 1994). The bilinear factor analysis model can be described by Equation (1), where the measured concentration of species (x_{ij}) can be expressed as the sum of the product of the source profile (f_{kj}) and its time series (g_{ik}).

$$x_{ij} = \sum_{k=1}^p g_{ik} f_{kj} + e_{ij} \quad (1)$$

where x_{ij} , g_{ik} , f_{kj} and e_{ij} are measured concentration of j th species in i th sample, contribution of k th source to i th sample, concentration of j th species in k th source and a residual matrix, respectively. PMF solves the bilinear Equation using the least square technique and by minimizing an objective function (Q) as in Equation (2), which is defined as the sum of the squared ratio of residuals (e_{ij}) and the measured uncertainty (σ).

$$Q = \sum_{i=1}^m \sum_{j=1}^n \left(\frac{e_{ij}}{u_{ij}} \right)^2 \quad (2)$$

where m and n denote the no. of samples and variables (species), respectively. While PMF does not require any priori information, the ME-2 implementation in PMF requires a priori information using the a -value approach, enabling the exploration of the rotational space efficiently. The advantage of ME-2 over PMF is that it has more control of rotations and full rotational space is accessible (Belis et al., 2019; Paatero and Hopke, 2009). Further, using the a -value approach, one or more factor profile/time series or any individual variable can be constrained using the scalar a -value varying from 0 to 1 according to the following Equations (3) and (4):

$$f'_{kj} = f_{kj} \pm a \times f_{kj} \quad (3)$$

$$g'_{ik} = g_{ik} \pm a \times g_{ik} \quad (4)$$

The ME-2 solver was applied to the measured data using the Source Finder tool (SoFi Pro v 6.8, Datalystica Ltd, Villigen, Switzerland) which provides an interface to efficiently control and explore the different rotational techniques in a smooth way (Canonaco et al., 2013) and used in Igor Pro v6.37 Software (Wavemetrics, Inc., Portland, OR, USA) for analysis.

2.3.1. OA source apportionment (SA)

HR PMF input matrix (197 ions) obtained from PIKA and UMR input matrix from SQUIRREL were combined from the variable (m/z 12 to m/z 300). The PMF was applied to the combined input matrix with 4839 data points (15 min averaged) and 397 variables (ions and UMR m/z species). The variables were down-weighted using the step function, weak variables ($S/N < 0.2$) with a factor of 10 and medium ($S/N < 2$) by a factor of 2, respectively (Paatero and Hopke, 2003). The CO₂⁺ related variables are excluded from PMF analysis so that its intensity is not overweighted. Elemental ratios (O/C, H/C, OM/OC and N/C) of PMF factors were calculated using the software APES v 1.09 (Sueper, 2018) in Igor Pro v

6.37 (Wavemetrics, Inc., Portland, OR, USA).

In this campaign, we have used combined HR (ions from m/z 12 to m/z 100) and UMR (from m/z 100 to 300) spectra for our PMF analysis measured using HR-ToF-AMS. The advantage of using high $m/z > 120$ is to get polyaromatic hydrocarbons (PAHs) to identify the coal combustion related markers.

The unconstrained PMF has been run on combined HR and UMR data from 3 to 8 factors. The Q_{res} decreased as the number of factors increased from 4 to 5 and the percentage relative change in the ratio Q/Q_{exp} has a very sharp decrease moving from 4 to 5-factor solution (Fig. S6 (a)). The detailed description of the selection of factors and the uncertainty estimate has been discussed in detail in supplementary. When increasing the factor from 5 to 6 (Fig. S6 (c)), the LVOOA was splitting into a mixed factor. So, the 5-factor solution has been identified as the optimum solution, including three primary factors, HOA, COA and SFC and two oxidized factors, LVOOA and SVOOA. In the 5-factor solution, HOA had high m/z 44 spectra after LVOOA and it got resolved in the 6-factor solution. This clean HOA factor from the 6-factor solution was used to constrain the 5-factor solution using a -value from 0 to 0.5. The detailed description of the selection of factors and the uncertainty estimate results by bootstrapping method has been discussed in detail in supplementary sections S1 and S3, respectively.

2.3.2. Xact elements source apportionment (SA)

The input data matrix of the elements measured with half-hourly time resolution was prepared by first filtering the elements based on the percentage of data points below their Minimum Detection Limit (MDL) (provided by manufacturer Cooper Environmental Services). Twenty-two elements (Al, Si, S, Cl, K, Ca, Ti, V, Cr, Mn, Fe, Ni, Cu, Zn, As, Se, Br, Rb, Sr, Sb, Ba and Pb) were found to have 80% of their data points above MDL and were used in the PMF input (Table S1). The error matrix was directly taken from the Xact 625i software, which reports the uncertainty for every sampled data, based on spectral deconvolution uncertainty and the measurement uncertainty (Tremper et al., 2018). The input matrix consists of 1861 data points (same time resolution as raw data) and 22 elements. The down weighting of variables with $S/N < 2$ was done by replacing the individual value with the corresponding $2/SNR$ value. The down weighting of individual cell values has the advantage of not affecting the data period with high SNR in a variable (Rai et al., 2020b).

PMF was applied to the elemental dataset, the completely unconstrained PMF was run from 3 to 11 factors. A very sharp decrease in the Q/Q_{exp} ratio was observed on increasing the number of factors from 6 to 7 (21%) (Fig. S7 (a)). So, 7-factor solution was selected as the optimum solution. Further, the profile, time series, Q_{res} and scaled_{res} were analyzed (details in supplementary section S2). In unconstrained PMF 8-factor solution, dust related two factors: Al-Si and Ca-Sr rich, Cl-rich, Zn-rich, S-rich, K-Br, Pb-rich, Cu-rich were resolved. Further exploring the 8-factor unconstrained solution, the two dust factors were highly correlated and a clean non-exhaust factor which was not resolved in 8-factor solution (Fig. S7 (b)) but in 11-factor solution (Fig. S7 (c)) as the Q_{res} and UEV (unexplained variation) was supporting the Ba-Fe (markers of non-exhaust source and also the diurnal having high concentrations at traffic hours) to be resolved in 11-factor solution (Fig. S7 (c)). The PMF was run for 20 seeds for 8-factor solution before constraining the factor. The 8-factor unconstrained solution was constrained with the clean non-exhaust (from 11-factor solution) profile, from a -value 0 to 1. The detailed description of the selection of factors and the uncertainty estimate results by bootstrapping method has been discussed in detail in supplementary sections S2 and S3, respectively.

2.4. Uncertainty estimate of OA and elemental ME-2 SA results

Bootstrapping is a widely used method in ME-2 for estimating uncertainty and determining the statistical stability of solutions (Brown et al., 2015; Rai et al., 2020b). Bootstrapping analysis estimates the

observed data's statistical properties by drawing multiple random samples with replacement from the original data set. Further, it creates several bootstrap distributions with identical dimensions as the original dataset and computing the desired statistics from each bootstrap distribution to capture the statistics' dependency with random variations in the data. A detailed description of the bootstrapping technique is discussed in Paatero et al. (2014). The methodology followed in the paper has been adopted by many previous studies (Rai et al., 2020b; Stefenelli et al., 2019). The uncertainty estimate was performed for 1000 bootstrap runs on both the OA and elemental SA results obtained by ME-2. The bootstrap run was performed for 5-factor solution with only the HOA factor constrained and the remaining factors were unconstrained. The a-value for constrained factor was randomly and independently initialized from 0 to 0.5 with a step size of 0.1. Each bootstrap run is started from a different initialization point as a-value was randomly varied; it implies that this methodology also includes the investigation of seed-based variability (Stefenelli et al., 2019).

Similarly, for the elemental ME-2 result, the bootstrap analysis was done for 8-factor solution with only a non-exhaust factor that was constrained. The a-value was initialized randomly between 0 and 1 with a delta of 0.1. The uncertainty estimate results are described in detail in the supplementary section S3. In summary, bootstrap analysis for OA resulted in 971 runs out of 1000 as unmixed with an average a-value of 0.259 for the constrained HOA factor. While the bootstrap analysis for elements, 605 runs out of 1000 classified as unmixed solutions with an average a-value of 0.534 for constrained non-exhaust solutions.

2.5. Black carbon (BC) source apportionment (SA)

The BC data at seven different wavelengths from Aethalometer helps to differentiate sources of BC based on their absorbance in different wavelength ranges of light. BC from biomass burning has high absorbance in the ultraviolet and visible range than BC from fossil fuel (traffic) (Ganguly et al., 2005; Sandradewi et al., 2008). A model based on absorption angstrom exponent (AAE) is used where AAE is calculated by Eq. (5).

BC SA is performed on the multiwavelength aethalometer (AE-33) derived data using the aethalometer model discussed by Sandradewi et al. (2008). The aethalometer model is widely used to separate the BC from wood burning and traffic emissions in sites where no other BC major sources are present (Dumka et al., 2018; Sandradewi et al., 2008; Tobler et al., 2020; Zotter et al., 2017). The model separates the traffic and wood burning by considering that the BC from wood-burning absorbs strongly at ultraviolet and lower visible range than traffic emission BC.

The absorption Angstrom exponent (AAE) as expressed in Equation (5), is calculated based on the absorption coefficients 'b' at 470 nm (b_{470}) and 950 nm (b_{950}).

$$AAE = \frac{\ln\left(\frac{b_{470 \text{ nm}}}{b_{950 \text{ nm}}}\right)}{\ln\left(\frac{950}{470}\right)} \quad (5)$$

Various studies have used different values for AAE for traffic (AAE_{FF}) and AAE for biomass burning (AAE_{BB}) (Dumka et al., 2018; Rupakheti et al., 2017; Sandradewi et al., 2008; Tobler et al., 2020; Zotter et al., 2017). AAE_{BB} is used to represent the AAE of the BC emitted from complex biomass sources. The present study uses AAE_{FF} and AAE_{BB} reported in a recent study, Tobler et al. (2020) performed the BC SA in Delhi using the AAE_{FF} value of 0.9 and a lower AAE_{BB} value of 1.5. Details of the selection of AAE_{FF} and AAE_{BB} can be found in Tobler et al. (2020).

2.6. Back trajectory analysis using concentration weighted trajectory (CWT)

Back trajectory analysis is used to estimate the possible central path

or source from which the air parcel travels to the receptor site at a given time. Back trajectory analysis was performed by (Hybrid Single Particle Lagrangian Integrated Trajectory v4.1 (HYSPPLIT) (Draxler, 2020) software using the weekly Global Data Assimilation System (GDAS) files (<ftp://arlftp.arlhq.noaa.gov/pub/archives/gdas1>) with a $1^\circ \times 1^\circ$ resolution. The back trajectories were calculated for 72 h with 3-h time resolution averaged data for an altitude of 100 m above ground level (AGL) (Rai et al., 2020b). Concentration weighted trajectory (CWT) back trajectory analysis identifies potential transport of pollution over a large geographical area and using ambient concentrations with back trajectories and residence time information to identify air parcels responsible for high concentrations observed at the receptor site (Fleming et al., 2012; Petit et al., 2017).

The calculated back trajectories were weighted with the 3-h averaged factor time series resolved from the SA studies of organics and elements. The average CWT is calculated using Equation (6), as described by (Rai et al., 2020b):

$$CWT_{ij} = \frac{1}{T_{ij}} \sum_{k=1}^N C_k T_{ijk} \quad (6)$$

Where latitude and longitude are represented by i and j respectively, CWT_{ij} is the average weighted concentration in $\mu\text{g}\cdot\text{m}^{-3}$ in the ij th cell, N is total trajectories and C_k is the measured factor concentration of trajectory k and T_{ijk} is the residence time of trajectory k in ij th cell.

3. Results and discussion

3.1. PM_{2.5} mass concentration

The PM_{2.5(eq)} concentration is the sum of NR-PM_{2.5} (Org, SO₄²⁻, NO₃⁻, NH₄⁺ and Cl⁻), elements and BC and their hourly variation is shown in Fig. 1 (a). For the common period, the hourly average PM_{2.5(eq)}, NR-PM_{2.5}, PM_{El} and BC are 28.7 ± 13.2 (8–94) $\mu\text{g}\cdot\text{m}^{-3}$, 14.1 ± 8.1 (3–49) $\mu\text{g}\cdot\text{m}^{-3}$, 9.7 ± 9.8 (1–87) $\mu\text{g}\cdot\text{m}^{-3}$ and 5 ± 3.9 (0.7–29) $\mu\text{g}\cdot\text{m}^{-3}$, respectively. The PM_{2.5(eq)} mass includes elements, organics, inorganics, and BC representing 34%, 28%, 21% and 17%, respectively. The hourly PM_{2.5(eq)} concentration correlates strongly with the EBAM PM_{2.5} (slope = 0.51 and R = 0.8) (Fig. S1). The time series is dominated by elements as several dust storms characterized by high Si, Al, and Fe concentrations occurred during the campaign (June 11th, 16th, 17th, and 21st, 2020). Organics dominate the NR-PM_{2.5} concentration, followed by sulfate with a combined contribution of 83% to the total NR-PM_{2.5}. The OA diurnal has a high concentration period in the daytime for long hours, indicating the significant contribution from the secondary sources but also has a nighttime peak of ~ two times higher concentration than average daytime concentration, indicating contribution from the combustion sources, as shown in Fig. 1 (b). The high nighttime concentration further indicates the decrease in the planetary boundary layer (PBL) and enhanced local emissions during nighttime and early morning. Sulfate has a less diurnal variation (Fig. 1 (b)) among all NR-PM_{2.5} species, but comparatively higher concentration during daytime which could be attributed to a combination of high daytime photochemical formation rates at high temperature and long-range transportation of secondary sulfate aerosols (Gani et al., 2018).

NO₃⁻, Cl⁻ and NH₄⁺ showed similar diurnal patterns having a high concentration around 9:00 LT (local time). Both the ammonium nitrate and ammonium chloride are semi-volatile which can be vaporized due to high temperatures (sunrise) in summer. The nitrate has a U type minimum around noon indicating vertical mixing. The chloride diurnal becomes completely flat after the peak at 9:00 LT suggests complete dilution due to an increase in PBL.

The crustal dust-related elements dominated the elemental concentration with Si contributed 31% of total elemental mass followed by S with 19% contribution (Fig. 1 (c)). Elements showed a strong diurnal pattern (Fig. S3). The diurnal maxima to minima ratio for elements were

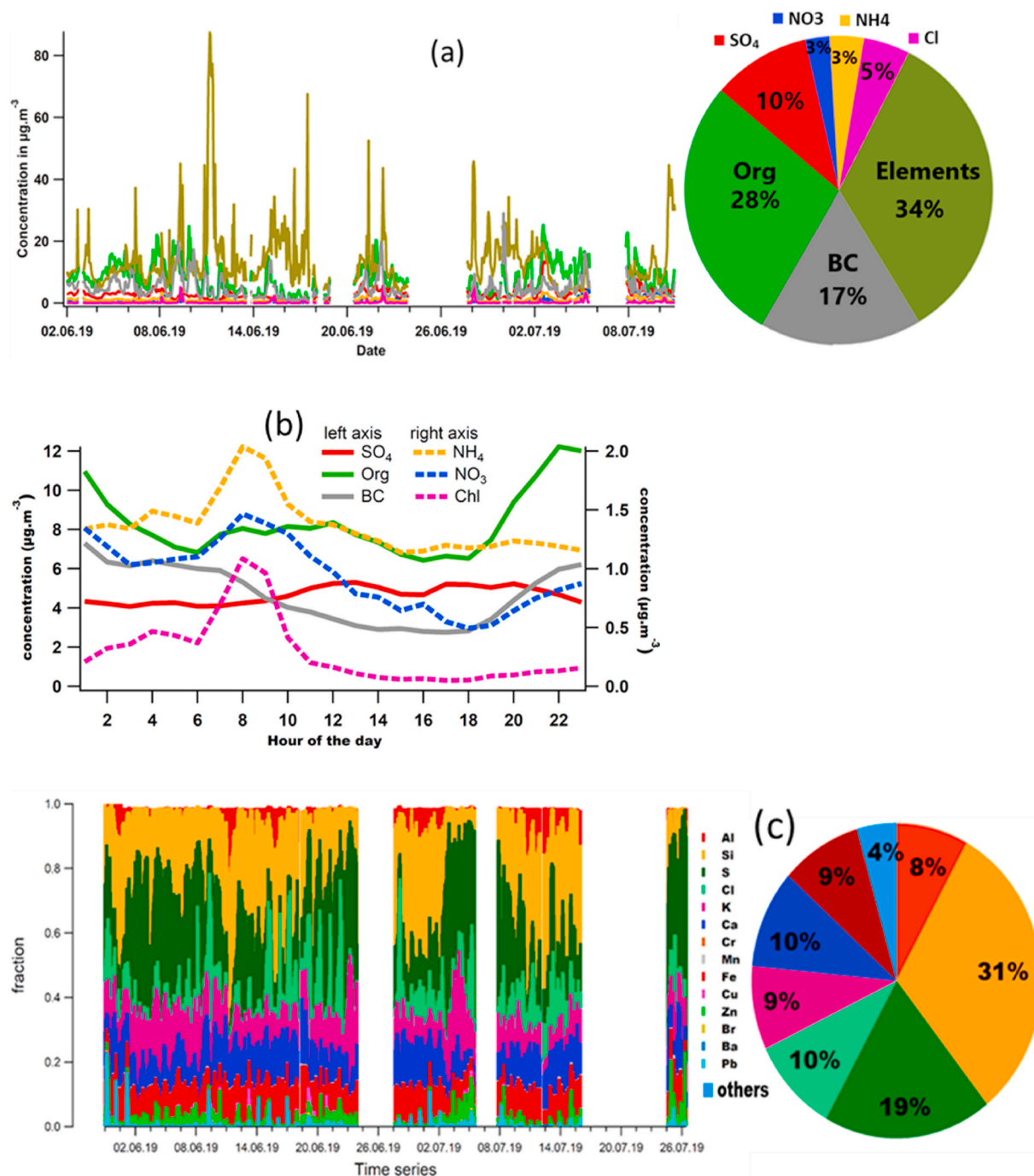


Fig. 1. (a) Fractional composition of PM_{2.5(eq)} and relative contribution of PM_{2.5(eq)} species (Org, SO₄²⁻, NO₃⁻, NH₄⁺, Cl⁻, PM_{El} and BC) and (b) diurnal variation of Org, SO₄²⁻, NO₃⁻, NH₄⁺, Cl⁻ and BC, and (c) contribution weighted time series, and relative contribution of elements measured by Xact.

very high with Pb (14), Cd 402 (14), Cu (8.1), Cl (7), and As, Se, Sn, and Br about three and these elements have sharp peaks after midnight to early morning indicating the presence of local emissions. Al, Si, K and Ca have diurnal maxima to minima ratio around two. These all are peaking during daytime except K indicating the contribution of regional sources to these elements. Several high episodic peaks of chloride have two distinct sharp diurnal peaks between 04:00 LT and 07:00 LT, with a maximum concentration of 37 µg m⁻³.

The BC has a sharp diurnal variability, with a high concentration early morning and the nighttime peak concentration around three times higher than midday-time hours (Fig. 1 (b)). The high diurnal variation of BC can be explained by the local BC sources, including the major ring road near the sampling site with heavy load vehicles (trucks). These

trucks are often restricted to only passing through Delhi at night (Guttikunda and Calori, 2013). The BC concentration is five times lower than that reported in winter at the same site by Lalchandani et al. (2021). The percentage contribution of BC to the total PM is high in summer compared to winter and is consistent with previous studies in Delhi (Gani et al., 2018; Tobler et al., 2020).

3.2. Organic aerosol (OA) source apportionment (SA)

The SA of OA resulted in clean three primary factors; HOA, SFC and COA and two oxidized factors; LVOOA and SVOOA. The factors are described in detail as following:

HOA – Fig. 2 (a) shows the mass spectral pattern of HOA, which is

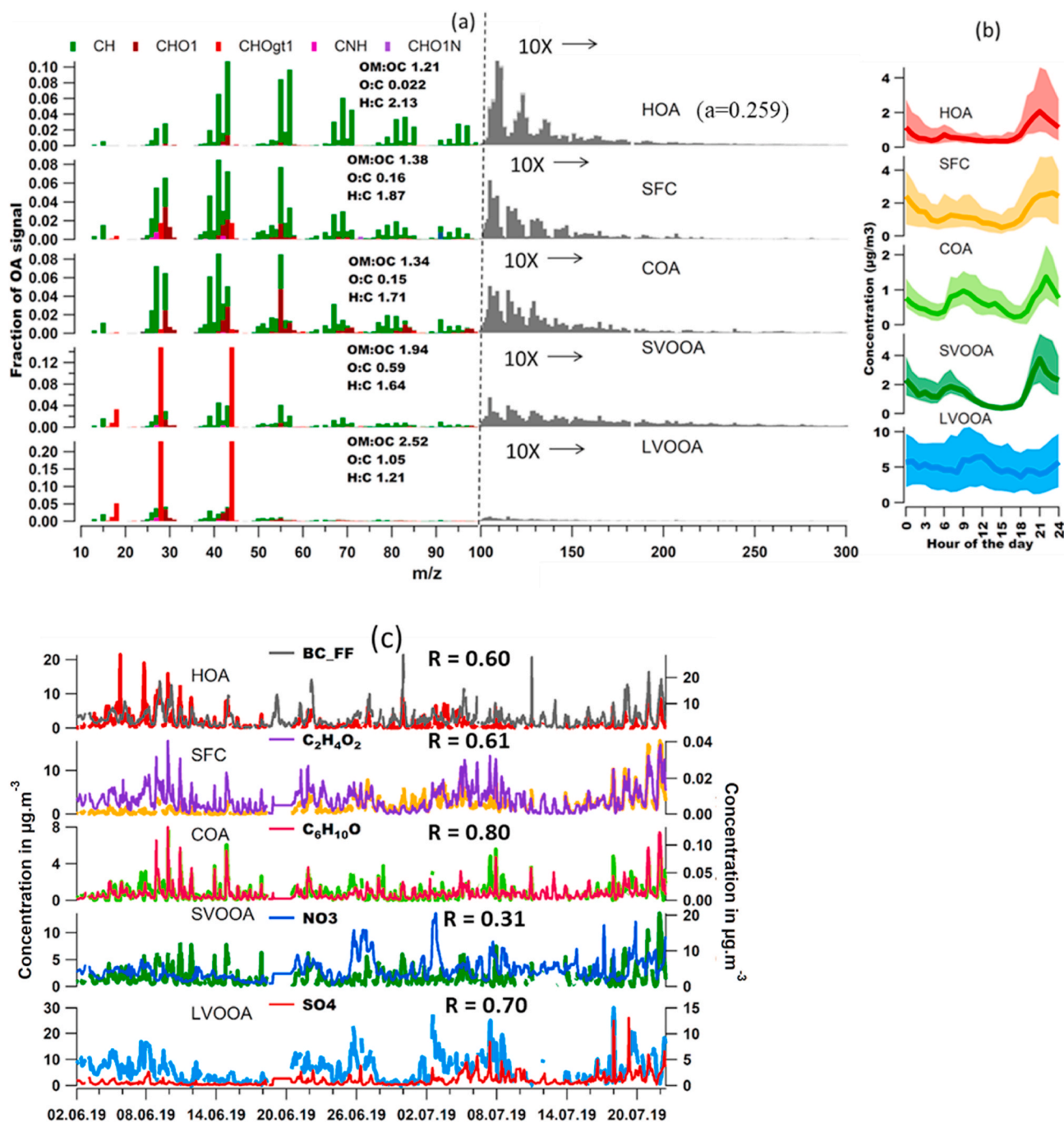


Fig. 2. (a) PMF mass spectra (top left), (b) diurnal variation of mass concentration (top right) and (c) time series of OA factors (left axis) with external tracers (right axis).

characterized by the significant hydrocarbon ion series C_nH_{2n-1} and C_nH_{2n+1} , particularly m/z 43 (C_3H_7), 55 (C_4H_7), 57 (C_4H_9), 69 (C_5H_9), 71 (C_5H_{11}), 81 (C_6H_9), 95 (C_7H_{11}) and 98 (C_7H_{14}) and are similar to previously reported HOA spectra at various urban sites (Crippa et al., 2013; Hayes et al., 2013; Lalchandani et al., 2021; Mohr et al., 2012; Ng et al., 2010; Tobler et al., 2020). The HOA factor is related to fossil fuel combustion which includes diesel exhaust, typically dominated by recondensed engine lubricating oil and consists mainly of n-alkanes, branched alkanes, cycloalkanes and aromatics (Canagaratna et al., 2004). The time series of HOA correlates well with CO ($R = 0.80$), NO_x and BC_FF ($R = 0.6$), as shown in Fig. 2 (c). The average mass concentration of HOA is $1.5 \pm 2.3 \mu\text{g m}^{-3}$ and its contribution is 12.3% to total OA mass. Lalchandani et al. (2021) reported the average HOA

concentration in winter to be $26.7 \mu\text{g m}^{-3}$ at IITD, while Tobler et al. (2020) found it $15.6 \mu\text{g m}^{-3}$ at another site in Delhi and reported a contribution of around 20% to the total OA mass. The studies were not able to separate the cooking emissions from the HOA in winter. The diurnal variation shown in Fig. 2 (b) has a small rush hour peak in the morning and a very high nighttime peak due to the heavy-duty trucks allowed at nighttime in Delhi and the major road close to the sampling site. The spectral intensity ratio of m/z 55 to m/z 57 is less than one and it has the highest elemental H: C ratio of 2.13 across the factors.

SFC – The factor as shown in Fig. 2 (a) is characterized by high spectral intensities at m/z 29 (CHO), 39 (C_3H_3), 41 (C_2HO), 50 (C_4H_2), 51 (C_4H_3), 53 (C_4H_5), 77 (C_6H_5), 91 (C_7H_7) and high m/z PAH's (105, 107, 115, 128, 152, 165, 178, 189, and 202), which are widely used as a

marker for biomass and coal combustion (Dall'Osto et al., 2013; Hu et al., 2013). It also contributes to other aromatic compounds including nitrogen compounds (C_2H_4N , CH_3NO , C_3H_7NO , C_3H_9NO). The average mass concentration of SFC is $2 \pm 2.2 \mu\text{g m}^{-3}$ and it contributes 16.2% to total OA mass. Lalchandani et al. (2021) found 2 SFC factors at the same site in winter, while Tobler et al. (2020) reported one SFC factor for another location in Delhi with an absolute concentration around $25 \mu\text{g m}^{-3}$ and contribution to total OA mass was 26% and 34%, respectively. The SFC was high in the nighttime from 21:00 LT to 3:00 LT, as shown in Fig. 2 (b) indicating nighttime burning activities and influence of boundary layer height. The time series is correlated well with CO ($R = 0.85$) which is a tracer for incomplete combustion (Lanz et al., 2007), m/z 60 as shown in Fig. 2 (c) and BC_{BB} ($R = 0.6$) (Alfarra et al., 2007) both of which indicate biomass burning especially coal and with aromatics m/z 77 ($R = 0.81$) and m/z 91 ($R = 0.76$) which are associated with coal combustion (Wang et al., 2017). Fig. 4 (a) shows the source region to be transported from the south east direction and close to the sampling site. The total spectral intensity of m/z 60 and m/z 73 is significantly less than in winter, so there is no distinct peak signal at m/z 60 or m/z 73 in any of the PMF factors.

COA – The COA profile is as shown in Fig. 2 (a), characterized by prominent signals at m/z 27 (C_2H_3), 29 (C_2H_5), 41 (C_2HO), 55 (C_3H_3O), 57 (C_3H_5O), 71 (C_4H_7O), 81 (C_5H_5O), 83 (C_5H_7O), 84 (C_5H_8O), and 98 ($C_6H_{10}O$) (Fröhlich et al., 2015; He et al., 2010; Mohr et al., 2012). It is consistent with a high degree of oxygenation of fatty acids, a major constituent of COA (Mohr et al., 2012). $C_6H_{10}O$ has been widely used as a distinct marker to distinguish COA from HOA and its relative contribution is around 70% across the factors (Sun et al., 2016). The ratio of intensity at m/z 55 over that of m/z 57 is 6.4 and that of m/z 41 to m/z 43 is 1.7 is supporting the factor to be from cooking source (Crippa et al., 2013a,b; Wang et al., 2017). The diurnal concentration of COA has a large peak around 9:00 LT and a small peak around 15:00 LT during day and a clear peak at night, as shown in Fig. 2 (b) (Allan et al., 2010). Similar diurnal behaviors of COA have been observed at another site in Delhi (Cash et al., 2020). The time series of the factor is also correlated with VOC ion at m/z 45 (C_2H_5O) ($R = 0.6$) and m/z 79 (C_6H_7) ($R = 0.4$) used as a marker for cooking emissions (Crippa et al., 2013a,b). Only a recent SA study in Delhi has been able to separate the HOA and COA factor (Cash et al., 2020) with rest two of the studies focused on winter and one for all the season (Bhandari et al., 2020; Lalchandani et al., 2021; Tobler et al., 2020) were unable to resolve the COA source. The average measured mass concentration of COA is $0.9 \pm 1 \mu\text{g m}^{-3}$ with a mass fraction of 7.3% of total OA and the time series correlated well with m/z 98 ($C_6H_{10}O$) with $R = 0.80$ as shown in Fig. 2 (c).

SVOOA and LVOOA – Two oxygenated factors resolved as LVOOA and SVOOA dominate the total OA mass concentration with 49.1% and 15.2% contribution, respectively. These two factors are characterized with high spectral intensity at m/z 44 (CO_2^+), i.e., 64.5% for LVOOA and 22% for SVOOA across the factors, as shown in Fig. 2 (a). The LVOOA does not have any significant signal from m/z higher than 44 but the SVOOA has a clear contribution from other hydrocarbons. The LVOOA factor has a high O: C ratio of 1.05, followed by SVOOA with an O: C of 0.59. Both the O: C values are quite high compared to those reported in winter at the same site with O: C of 0.49 and 0.33 for LVOOA and SVOOA, respectively (Lalchandani et al., 2021). The contribution of OOA sources to the total OA mass is around 50% in winter and 56% in summer in previous studies (Bhandari et al., 2020; Lalchandani et al., 2021; Tobler et al., 2020). The time series of LVOOA is correlated well with SO_4^{2-} and elemental sulfur ($R = 0.7$) while that of SVOOA is correlated with NO_3^- ($R = 0.31$) as shown in Fig. 2 (c). The CWT plot Fig. 4 (a) shows that the possible source region of SVOOA to be more towards the south-east (SE) and less from the north-west (NW) while LVOOA has a high concentration from the SE direction. The LVOOA has not much diurnal variation indicating the source to be regional while the SVOOA has low concentration during the day and a high peak in the night at 21:00 LT which can be due to the combined effect of boundary

layer and condensation of gas phase pollutants as shown in Fig. 2 (b).

3.3. Source apportionment (SA) of Xact elements

The detailed description of factors identified from the SA of elements are as follows:

Non-exhaust– The factor is mainly characterized by a high relative contribution of Ba (100%) and Cr (83%). Mn, Fe, and Ni contributed around 50% while Ti, V and Sb contributed to this factor between 10 and 20% as shown in Fig. 3 (a). Fe represented a mass fraction of 60% and Ca about 20% in this factor. Fe, Ba, Cr, Mn, Ni and Sb have been used as tracers for brake and tyre wear (Rai et al., 2020b; Visser et al., 2015). Fe and Ba can be regarded as chemical tracers for the traffic-related source (exhaust and non-exhaust) (Chang et al., 2018). The factor's time series correlates moderately with NO_x ($R = 0.5$) as shown in Fig. 3 (c). The diurnal concentration peaks as shown in Fig. 3 (b) at traffic hours from 7:00 to 11:00 LT and at 22:00 LT. The concentration was high from midnight to early morning as HDV is more during this time. The non-exhaust factor contributed 7.2% to the total elemental mass and its average mass concentration is $1 \pm 1.3 \mu\text{g m}^{-3}$.

Dust– The relative contribution of elements to this factor are shown here in % in parenthesis: Al (98%), Si (94%), K (28%), Ca (83%), Ti (67%), V (70%), Mn (32%), Fe (36%), Ni (35%), Rb (63%), Sr (92%) and Sb (16%) however, the mass is dominated by Si (53%), Al and Ca (20%) as shown in Fig. 3 (a). Al, Si, Ca, Sr, and Ti is widely used as a tracer for dust-related sources (Pant and Harrison, 2012; Rai et al., 2020b; Sharma et al., 2016; Sun et al., 2019). The CWT plot shows that it is transported from long-range in the south-west (SW) direction from the deserts of Rajasthan (Fig. 4 (b)). Multiple high loading dust-storms were observed in June which can be seen in several peaks in Fig. 3 (c). Other possible sources of dust, such as road dust and weathering, as well as rock erosion may have contributed to the factor. The low Enrichment factor (EF) values (Supplementary section S3) of Al, Si, Ti and Sr are consistent with the upper continental crust composition (Rudnick and Gao, 2003). The dust factor dominated the PMF factors with 52.5% of the total elemental mass and its average mass concentration is $7.5 \pm 7.4 \mu\text{g m}^{-3}$ with a maximum concentration of $86 \mu\text{g m}^{-3}$ during the dust storms. The diurnal variations indicate daytime maxima and high concentrations as shown in Fig. 3 (b). The time series of dust factor also increases with increasing temperature and decreasing RH (Fig. S2).

Cl-rich– The relative percentage contribution is dominated by Cl (96%) and Br (28%), while the mass fraction is explained by Cl with 90% of the mass as shown in Fig. 3 (a). Several high episodes of Cl have been found during winter in Delhi (Gani et al., 2019; Rai et al., 2020b; Tobler et al., 2020). Similar episodes were found in summer. Cl is used as a tracer for garbage burning and coal combustion. Anthropogenic Cl emissions are primarily in the form of HCl which can be emitted from the treatment of carbon steel products in the steel industry. The CWT plot shown in Fig. 4 (b) shows that most of the source is in the NW direction from Punjab, Haryana and Pakistan. There are many small and medium scale metal processing industries in Punjab, Haryana and Pakistan. The good correlation between the time series of NH_4^+ and Cl^- indicates that gaseous ammonia is sufficient to react with the HCl and the secondary particles of NH_4Cl are formed. The diurnal has a sharp peak at around 7:00 LT and has high concentrations at around 3:00 LT to 7:00 LT while it is entirely flat during the daytime hours, as shown in Fig. 3 (b). The other possible sources of HCl may be from the combustion of polyvinyl chloride, garbage burning, coal and biomass burning (Dall'Osto et al., 2013; Gani et al., 2018). The Cl-rich factor contributed 10.7% to the total elemental mass with an average mass concentration is $1.5 \pm 3.9 \mu\text{g m}^{-3}$ and a maximum concentration of $42 \mu\text{g m}^{-3}$ during Cl episodes. The time series of the Cl-rich factor is well correlated with AMS Cl^- with R around 0.8 as shown in Fig. 3 (c).

SFC I– The relative percentage contribution in the factor was K (63%), As and Rb (40%) and Se and Sb (around 20%) while the total mass fraction of the factor is dominated by K (72%) as shown in Fig. 3

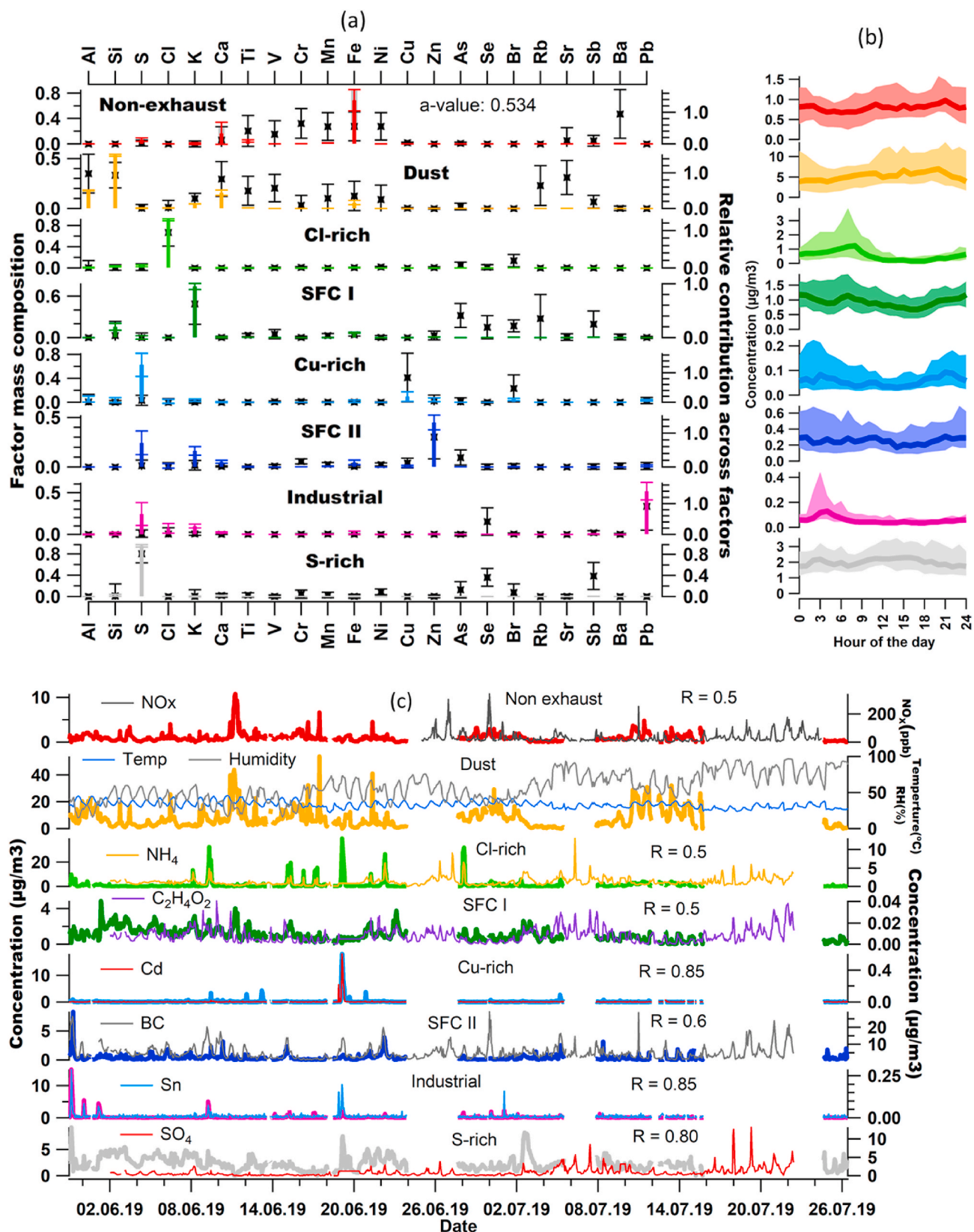


Fig. 3. (a) Source profiles of the 9-factor PMF results as the mean of 605 good solutions ± 1 SD from the bootstrap analysis. The left axis represents the factor mass composition (indicated as colored bars); the right axis represents the relative contribution of the factor to each variable (shown as black markers), (b) diurnal variation of mass concentration (top right) and (c) time series of the factors of elemental PMF result (left axis) with external tracers (right axis).

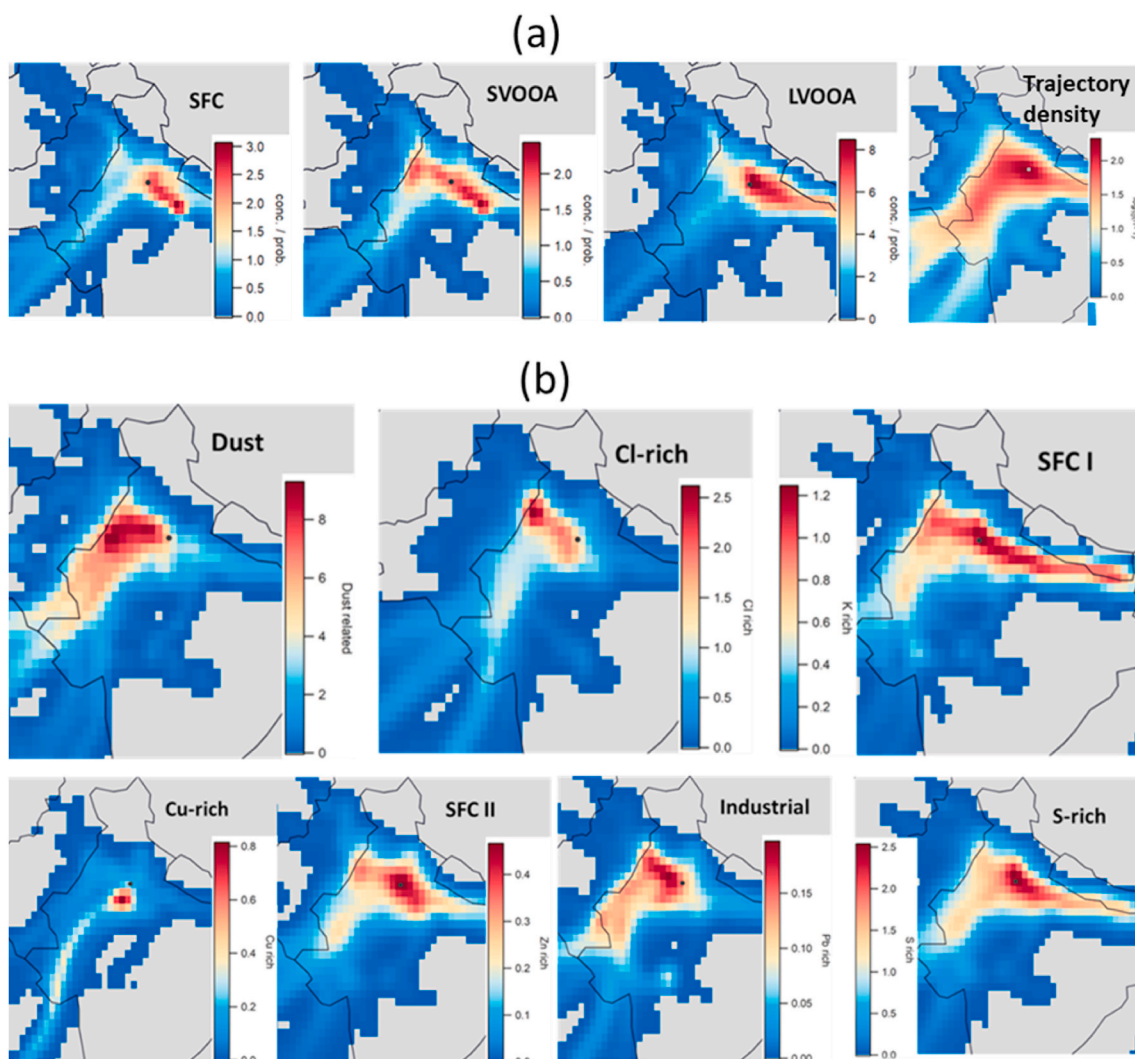


Fig. 4. (a) CWT plots for OA PMF factors SFC, SVOOA, LVOOA and trajectory density (shows the occurrence of Back Trajectory endpoints which fall into a particular cell), respectively and (b) CWT plots for elemental PMF factors dust related, Cl-rich, SFC I, Cu-rich, SFC II, industrial and S-rich, respectively.

(a). K is widely used as a marker for biomass burning worldwide (Jai-prakash, 2017; Rai et al., 2020b; Yu et al., 2018). Rb and As have been reported in residual crop burning (Lin et al., 2018). Alkali metals in the biomass structure are released to the gas phase and possibly react to form chemical species, e.g., KCl (Hindiyarti, 2007). While in winter, the burning of rice stock and stubble has created several pollution events from Punjab and Haryana mainly due to wind from the NW direction (Bhandari et al., 2020). It seems that now the burning of wheat stubble and biomass has been started affecting Delhi supported by the wind direction in summer from the east and northeast (NE) (west Uttar Pradesh). Mechanized harvesting leaves more residue in the field in the form of straw and stubbles for rabi and Kharif crops growing season, which are burnt to clear the area for subsequent crops. The CWT plots in Fig. 4 (b) show the highest concentration from an eastward direction near west Uttar Pradesh supporting the factor. The time series of the SFC I factor is well correlated with the time series of levoglucosan $C_2H_4O_2$ (m/z 60) of AMS ($R = 0.5$) as shown in Fig. 3 (c) which is a primary marker for biomass burning emissions (Simoneit et al., 1999). The other anthropogenic sources of K, As, Se and Sb are from coal/wood burning. The mass concentration has a diurnal peak around 7:00 LT and generally higher during the night and early morning (6:00 to 8:00 LT) as shown in Fig. 3 (b). The average measured mass concentration of the SFC I factor is $1.1 \pm 0.7 \mu g m^{-3}$ and its relative contribution is 7.6%.

Cu-rich– The relative percentage contribution is dominated by Cu

(98%) and Br (22%) as shown in Fig. 3 (a). The time series of Cu correlates with Cd as shown in Fig. 3 (c) with R around 0.85. The Cu–Cd is found to be co-emitted from the Cu–Cd alloy manufacture industry (Rai et al., 2020b). The CWT plot in Fig. 4 (b) predicts the source contribution from the SW direction. There is a Manesar industrial area and a landfill site with waste to energy conversion plant in Gurgaon, Haryana suggests a possible source might be industrial waste burning (Cu containing materials, i.e., wires, etc.) (Rai et al., 2020b). In winter (Rai et al., 2020b), found a similar Cu-rich factor but in the northeast direction. The diurnal shown in Fig. 3 (b) shows a peak at 3:00 LT and then during the day it is entirely flat and again has a peak around 23:00 LT. The Cu-rich factor contributed 1.5% to the total elemental mass with an average mass concentration of $0.2 \pm 1 \mu g m^{-3}$.

SFC II– The relative percentage contribution is dominated by Zn (85%) with As (27%). The total mass fraction of the factor is characterized by Zn (42%), S (30%) and K (16%) as shown in Fig. 3 (a). Zn, As, S and K are the tracers for coal combustion (Nalbandian, 2012; Sharma et al., 2016). Zn can also be emitted from traffic related, waste incineration and industrial burning (Pant et al., 2015). The CWT plot in Fig. 4 (b) shows that SFC II is local, while SFC I is regional. The time series of the SFC II factor is correlated well with BC ($R = 0.6$). The diurnal concentration is low during the day and high during the night and early morning with a sharp peak at 7:00 LT as shown in Fig. 3 (b). The SFC II factor contributed 2.9% across the factors and its average mass

concentration is $0.4 \pm 0.6 \mu\text{g m}^{-3}$.

Industrial– The relative percentage contribution is dominated by Pb (93%) with Se (41%). The total mass fraction of the factor is dominated by Pb with 68% as shown in Fig. 3 (a). Pb is used as a tracer for metal processing plants and lead-acid battery manufacturing and recycling (CPCB, 2016), steel, plastic and pigment production (Li et al., 2012) and non-ferrous metal smelting (Jeong et al., 2016). The CWT plot in Fig. 4 (b) shows that the source's high concentration region is quite consistent during both summer and winter in NW directions in Punjab and Haryana. There are various small and medium scale metal processing industries in that region (Rai et al., 2020b). The time series of the industrial factor correlates well with Sn ($R = 0.85$) as shown in Fig. 3 (c) which can be co-emitted with Pb from the lead-acid battery manufacturing and recycling process. As shown in Fig. 3 (b), the diurnal concentration has a sharp peak around 4:00 LT and completely flat during the day. The Industrial factor contributed 1.4% to the total elemental mass and its average mass concentration is $0.2 \pm 0.9 \mu\text{g m}^{-3}$.

S-rich– The relative contribution of elements dominating the factor is S (85%), Se and Sb (40%), As and Br (15%), as shown in Fig. 3 (a). The total mass fraction of the factor is mainly explained by S (98%) as shown in Fig. 3 (a). S, As, Se and Sb are widely used as a marker for coal combustion from thermal power plants (Nalbandian, 2012). Br-based products are used to reduce mercury emissions from coal-based thermal power plants (Liu et al., 2007). The CWT plot as in Fig. 4 (b) shows high concentrations from the SE direction of the sampling site. There are 11 coal-based thermal power plants in Delhi-NCR (Bhati et al., 2018). The diurnal variations shown in Fig. 3 (b) have peaks at 4:00 LT and 5:00 LT. However, it is flat during the day and had a high correlation with AMS SO_4^{2-} ($R = 0.8$) as shown in Fig. 3 (c) indicates that it is related to secondary sulfate in fly ash from coal combustion (Rai et al., 2020b). There is a massive difference in the coal and winter season observed in S-rich factors (Guttikunda and Jawahar, 2014). Guttikunda and Jawahar (2014) reported that around 80% of the PM from coal-based thermal power plants are secondary aerosols in Delhi-NCR during summertime. This factor is observed to contribute 16.2% to the total elemental mass and the measured average mass concentration is $2.3 \pm 1.3 \mu\text{g m}^{-3}$.

3.4. BC SA results and overview of OA and elemental SA results

The BC SA was dominated by fossil fuel (BC_FF) with 64.5% and biomass burning (BC_BB) only 35.5% to the total mass (Fig. S4). The average mass concentration of BC_FF and BC_BB is $3.34 \pm 2.9 \mu\text{g m}^{-3}$ and $1.69 \pm 1.2 \mu\text{g m}^{-3}$, respectively.

Comparing the SA results from the separate PMF study of organics and elements, The S-rich factor from elemental SA correlates well with the LVOOA factor ($R = 0.72$) from SA of organics and their diurnal concentration is similar to having high concentration during the day. The three SFC factors including two from elemental SA and one from OA SA demonstrated no correlation with each other and their diurnal behavior is also distinct as shown in Fig. S4.

3.5. Comparison with earlier studies in Delhi during the winter season

The hourly average NR-PM_{2.5} measured in the present study ($8.36 \mu\text{g m}^{-3}$) is 8–9 times lower than the measurements made during the winter season at IITD ($125.2 \mu\text{g m}^{-3}$, Lalchandani et al., 2021) and IITMDD (Tobler et al., 2020) sites in Delhi. The organics in the present study is 59% of total NR-PM_{2.5}, which is slightly higher than the values reported in previous studies for the winter season (Bhandari et al., 2020; Lalchandani et al., 2021; Tobler et al., 2020). Sulfate is the second dominant species and is 24% of NR-PM_{2.5} while it is only 10% in winter as reported in the previous three studies (Bhandari et al., 2020; Lalchandani et al., 2021; Tobler et al., 2020). In our summer study, the absolute concentration of Cl^- and NO_3^- was one-tenth of the concentration reported in these winter studies. This indicates that SO_4^{2-} dominates the

NR-PM_{2.5} in summer while the Cl^- and NO_3^- dominate the NR-PM_{2.5} in winter. The percentage contribution of NH_4^+ to the NR-PM_{2.5} varies between 8 and 12% in different seasons (Bhandari et al., 2020; Lalchandani et al., 2021; Tobler et al., 2020).

Our results show not only distinctly different characteristics of total PM_{2.5} concentrations but also the contribution of individual elemental mass to the total PM_{2.5} over Delhi during different seasons. For example, while in the present study, we find elements like Si (31%), S (19%), Cl and Ca (10%), K and Fe (9%) and Al (8%) to be dominating the total PM_{2.5} during summer, S (58.6%), Cl (21.4%), K (6.4%), Si (3.8%) and Al, Ca, Zn, Fe and Pb (around 2% each) were found to dominate the total PM_{2.5} during the winter season as reported by Rai et al. (2020b). The ratio of absolute concentration of winter to summer for Cl, Zn, Pb, S, K, Al, Fe, Ca and Si were 13.6, 2.9, 2.8, 2.6, 1.7, 0.6, 0.5, 0.33 and 0.3, respectively. The ratio shows that crustal elements: Al, Fe, Ca and Si were highly enhanced in summer while the elements emitted from the anthropogenic emissions: Cl, S, K, Pb and Zn were highly enriched in winter (Rai et al., 2020b).

The average concentration of HOA, SFC and OOA during summer was 18, 14 and 7 times lower than the OA SA study during winter at the same site (Lalchandani et al., 2021). The possible reason for the HOA ratio to be very high in winter is due to the separation of HOA and COA and the increased oxidation of primary aerosols in summer (Bhandari et al., 2020; Tobler et al., 2020). The difference between the percentage composition of POA and SOA in our study was 28.4% as compared to only 4% in winter indicating the dominance of secondary sources in summer. The source region predicted by the CWT model for HOA, SVOOA and LVOOA showed similarity while for SFC it changed from NW to SE direction due to the change in the wind pattern and other meteorological parameters (Lalchandani et al., 2021). The Dust and S-rich factors in percentage source contribution have increased significantly from winter to summer with a difference of 23.5% and 7%, respectively (Rai et al., 2020b). The contribution of the Cl-rich factor has decreased by 26.2% in summer while the rest of the factors are quite consistent in both seasons. The possible source region of Cu-rich, SFC-I and SFC-II had changed the directions from SE to SW, local to regional (NE) and NW to local while Cl-rich, Industrial and S-rich are consistent compared to the winter season (Rai et al., 2020b).

4. Conclusion

We present a complete chemical characterization of PM_{2.5} using state-of-the-art real-time online instruments such as HR-ToF-AMS, Xact625i and AE-33 from May 31, 2019 to July 26, 2019 in Delhi, India. The total-PM_{2.5(eq)} mass includes elements, organics, inorganics, and BC representing 34%, 28%, 21% and 17%, respectively. The high contribution of crustal elements to PM_{2.5} is noted during summer due to several dust storms affecting Delhi's air quality in this season.

Separate source apportionments are conducted using the PMF technique to unravel the sources of OA and elements in Delhi's atmosphere during the summer season. The OA source apportionment study yielded three primary factors with HOA (12.3%), SFC (16.2%) and COA (7.3%) and two oxygenated factors (SVOOA (15.2%) and LVOOA (49.1%)). For the first time, we quantify the contribution of cooking related activities towards POA over the study region during summer as previous studies carried out in the winter could not resolve the contribution of cooking-related this source. Both POA and OOA, were around 50% in the winter, which decreased to 35.2% and increased to 64.8% in the summer, respectively. While PMF using ME-2 analysis of elements provided 8 factors with Dust (52.5%) and S-rich (16.2%) dominated the sources followed by Cl-rich (10.7%), 2 SFC factors (10.5%), Non-exhaust (7.2%), Cu-rich (1.5%) and Industrial (1.4%).

The CWT analysis combined with the OA SA result shows that SFC and SVOOA over Delhi have sources mainly in the SE direction. In contrast, LVOOA has its potential source regions both in SE and NW directions. For elements, the CWT showed that the dust aerosols

originated from the west and SW directions from Rajasthan's desert area and are more regional and long-range transported. Our results show that the Industrial and Cl-rich sources such as small and medium metal processing industries in Punjab, Haryana and Pakistan contribute significantly to Cl in PM_{2.5} over Delhi. The origin of SFC-I was from NW and SE while local emissions influenced SFC-II. Cu-rich factor observed seems to get transported from SW direction as there are multiple metal alloy industries and incinerators. The S-rich factor was dominant from SE and east directions.

Although the absolute concentration of BC was found to be high in winter in earlier studies, the percentage contribution of BC to the total PM over Delhi is higher during summer than in winter. The SO₄²⁻ is found as the most dominant NR-PM_{2.5} inorganic species in summer while the Cl⁻ and NO₃⁻ are prevalent in the winter season in the previous studies in Delhi. We have resolved the source of COA over Delhi during summer only, which previous studies conducted during winter could not resolve which was possible perhaps due to lower concentrations of aerosols during summer than in winter. The other reason could be due to high anthropogenic emissions combined with the PBL effect causing a more significant mixing than winter, making it difficult to separate the sources due to the increased mixing. The HOA concentration was very high in winter compared to that in summer because of the separation of HOA and COA. Further, the increased oxidation of primary aerosols in summer and the boundary layer effect can also contribute to the HOA decrement. Our study reveals that, whereas crustal elements (Al, Fe, Ca, and Si) are significantly elevated, other elements associated with anthropogenic sources (Cl, S, K, Pb, and Zn) are reduced in PM_{2.5} concentrations over Delhi during the summer compared to the winter. The enhanced contribution of secondary sources can be observed in the summer as compared to the winter season for both OA and elements in PM. The possible source regions were also different for many sources such as dust, Cu-rich and SFC due to the drastic change in the meteorological conditions. The CWT plot of dust source dominated by multiple dust-storms in summer shows long-range air mass transport while it was found to be local and dominated by road dust in winter.

The secondary oxidized sources dominated both the OA and elements SA with 64% and 27% (dust not considered) during the summer. Therefore, for effective pollution control strategies in Delhi, it is crucial to control the precursors of secondary aerosols.

CRedit authorship contribution statement

Ashutosh K. Shukla: Methodology, Software, Validation, Formal analysis, Investigation, Writing – original draft, Writing – review & editing, Visualization. **Vipul Lalchandani:** Methodology, Formal analysis, Data curation, Validation, Writing – review & editing. **Deepika Bhattu:** Methodology, Validation, Writing – review & editing. **Jay S. Dave:** Investigation, Software, Data curation, Formal analysis, Writing – review & editing. **Pragati Rai:** Methodology, Validation, Writing – review & editing. **Navaneeth M. Thamban:** Formal analysis, Validation, Writing – review & editing. **Suneeti Mishra:** Formal analysis, Validation, Writing – review & editing. **Sreenivas Gaddamidi:** Investigation, Writing – review & editing. **Nidhi Tripathi:** Validation, Writing – review & editing. **Pawan Vats:** Investigation, Writing – review & editing. **Neeraj Rastogi:** Resources, Writing – review & editing. **Lokesh Sahu:** Resources, Writing – review & editing. **Dilip Ganguly:** Resources, Writing – review & editing. **Mayank Kumar:** Resources, Writing – review & editing. **Vikram Singh:** Resources, Writing – review & editing. **Prashant Gargava:** Resources, Writing – review & editing. **Sachchida N. Tripathi:** Conceptualization, Writing – review & editing, Supervision, Project administration, Funding acquisition.

Declaration of competing interest

The authors declare that they have no known competing financial interests or personal relationships that could have appeared to influence

the work reported in this paper.

Acknowledgements

The corresponding author gratefully acknowledges the financial support provided by the Department of Biotechnology (DBT), Government of India, to conduct this research under grant no.644 BT/IN/UK/APHH/41/KB/2016-17 dated 19th July 2017 and the financial support provided by Central Pollution Control Board (CPCB), Government of India to conduct this research under grant no. AQM/Source apportionment_EPC Project/2017.

Appendix A. Supplementary data

Supplementary data to this article can be found online at <https://doi.org/10.1016/j.atmosenv.2021.118598>.

References

- Alfarra, M.R., Prevot, A.S.H., Szidat, S., Sandradewi, J., Weimer, S., Lanz, V.A., Schreiber, D., Mohr, M., Baltensperger, U., 2007. Identification of the mass spectral signature of organic aerosols from wood burning emissions. *Environ. Sci. Technol.* 41 (16), 5770–5777. <https://doi.org/10.1021/es062289b>.
- Allan, J.D., Williams, P.I., Morgan, W.T., Martin, C.L., Flynn, M.J., Lee, J., Nemitz, E., Phillips, G.J., Gallagher, M.W., Coe, H., 2009. Contributions from transport, solid fuel burning and cooking to primary organic aerosols in two UK cities. *Atmos. Chem. Phys. Discuss.* 9 (5), 19103–19157. <https://doi.org/10.5194/acpd-9-19103-2009>.
- 2012 Battele, 2012. Environmental Technology Verification Report Cooper Environmental Services LLC † Xact 625 Particulate Metals Monitor. September 2012. <http://cooperenvironmental.com/>.
- Beig, G., Srinivas, R., Parkhi, N.S., Carmichael, G.R., Singh, S., Sahu, S.K., Maji, S., 2019. Anatomy of the winter 2017 air quality emergency in Delhi. *Sci. Total Environ.* 681, 305–311.
- Belis, C.A., Favez, O., Mircea, M., Diapouli, E., Manousakas, M.I., Vratolis, S., Gilardoni, S., Paglione, M., Decesari, S., Mocnik, G., Mooibroek, D., Salvador, P., Takahama, S., Vecchi, R., Paatero, P., 2019. In: European Guide on Air Pollution Source Apportionment with Receptor Models - Revised Version 2019. EUR 29816 EN, Publications Office of the European Union, Luxembourg. <https://doi.org/10.2760/439106>.
- Bhandari, S., Gani, S., Patel, K., Wang, D.S., Soni, P., Arub, Z., Habib, G., Apte, J.S., Hildebrandt Ruiz, L., 2020. Sources and atmospheric dynamics of organic aerosol in New Delhi, India: insights from receptor modeling. *Atmos. Chem. Phys.* 20 (2), 735–752. <https://doi.org/10.5194/acp-20-735-2020>.
- Bhati, P., Pathania, R., Phadke, P., Gupta, R.K., Ramanathan, S., 2018. Status of Thermal Power Stations in Delhi NCR OFF TARGET Centre for Science and Environment Design: Ajit Bajaj Production. Rakesh Shrivastava and Gundhar Das.
- Brown, S.G., Eberly, S., Paatero, P., Norris, G.A., 2015. Methods for estimating uncertainty in PMF solutions: examples with ambient air and water quality data and guidance on reporting PMF results. *Sci. Total Environ.* 518–519, 626–635. <https://doi.org/10.1016/j.scitotenv.2015.01.022>.
- Canagaratna, M.R., Jayne, J.T., Ghertner, D.A., Herndon, S., Shi, Q., Jimenez, J.L., Silva, P.J., Williams, P., Lanni, T., Drewnick, F., Demerjian, K.L., Kolb, C.E., Worsnop, D.R., 2004. Chase studies of particulate emissions from in-use New York City vehicles. *Aerosol. Sci. Technol.* 38 (6), 555–573. <https://doi.org/10.1080/02786820490465504>.
- Canonaco, F., Crippa, M., Slowik, J.G., Baltensperger, U., Prévôt, A.S.H., 2013. SoFi, an IGOR-based interface for the efficient use of the generalized multilinear engine (ME-2) for the source apportionment: ME-2 application to aerosol mass spectrometer data. *Atmospheric Measurement Techniques* 6 (12), 3649–3661. <https://doi.org/10.5194/amt-6-3649-2013>.
- Cash, J. M., Langford, B., Di Marco, C., Mullinger, N., Allan, J., Joshi, R., Heal, M. R., Joe Acton, W. F., Hewitt, N., Misztal, P. K., Drysdale, W., Mandal, T. K., Gadi, R., & Nemitz, E. (n.d.). Seasonal analysis of submicron aerosol in Old Delhi using high resolution aerosol mass spectrometry: Chemical characterisation, source apportionment and new marker identification. <https://doi.org/10.5194/acp-2020-1009>.
- Chang, Y., Huang, K., Xie, M., Deng, C., Zou, Z., Liu, S., Zhang, Y., 2018. First long-term and near real-time measurement of trace elements in China's urban atmosphere: temporal variability, source apportionment and precipitation effect. *Atmos. Chem. Phys.* 18 (16), 11793–11812. <https://doi.org/10.5194/acp-18-11793-2018>.
- CPCB, 2016. Air Pollution of Delhi: an Analysis. *ENVIS Centre on Control of Pollution (Water, Air, and Noise*, vol. 26. http://cpcbenvs.nic.in/envis_newsletter/Air_pollution_in_Delhi.pdf.
- Crippa, M., Canonaco, F., Slowik, J.G., El Haddad, I., Decarlo, P.F., Mohr, C., Heringa, M. F., Chirico, R., Marchand, N., Temime-Roussel, B., Abidi, E., Poulain, L., Wiedensohler, A., Baltensperger, U., Prévôt, A.S.H., 2013a. Primary and secondary organic aerosol origin by combined gas-particle phase source apportionment. *Atmos. Chem. Phys.* 13 (16), 8411–8426. <https://doi.org/10.5194/acp-13-8411-2013>.
- Crippa, M., Decarlo, P.F., Slowik, J.G., Mohr, C., Heringa, M.F., Chirico, R., Poulain, L., Freutel, F., Sciare, J., Cozic, J., Di Marco, C.F., Elsasser, M., Nicolas, J.B.,

- Marchand, N., Abidi, E., Wiedensohler, A., Drewnick, F., Schneider, J., Borrmann, S., Baltensperger, U., 2013b. Wintertime aerosol chemical composition and source apportionment of the organic fraction in the metropolitan area of Paris. *Atmos. Chem. Phys.* 13 (2), 961–981. <https://doi.org/10.5194/acp-13-961-2013>.
- Dall'Osto, M., Ovadiveite, J., Ceburnis, D., Martin, D., Healy, R.M., O'Connor, I.P., Kourtchev, I., Sodeau, J.R., Wenger, J.C., O'Dowd, C., 2013. Characterization of urban aerosol in Cork city (Ireland) using aerosol mass spectrometry. *Atmos. Chem. Phys.* 13 (9), 4997–5015. <https://doi.org/10.5194/acp-13-4997-2013>.
- Dall'Osto, M., Querol, X., Amato, F., Karanasiou, A., Lucarelli, F., Nava, S., Calzolari, G., Chiari, M., 2013. Hourly elemental concentrations in PM_{2.5} aerosols sampled simultaneously at urban background and road site during SAPUSS - diurnal variations and PMF receptor modelling. *Atmos. Chem. Phys.* 13 (8), 4375–4392. <https://doi.org/10.5194/acp-13-4375-2013>.
- DeCarlo, P.F., Kimmel, J.R., Trimborn, A., Northway, M.J., Jayne, J.T., Aiken, A.C., Gonin, M., Fuhrer, K., Horvath, T., Docherty, K.S., Worsnop, D.R., Jimenez, J.L., 2006. Field-deployable, high-resolution, time-of-flight aerosol mass spectrometer. *Anal. Chem.* 78 (24), 8281–8289. <https://doi.org/10.1021/ac061249n>.
- Draxler, R., 2020. HYSPLIT USER'S GUIDE. April.
- Drinovec, L., Močnik, G., Zotter, P., Prévôt, A.S.H., Ruckstuhl, C., Coz, E., Rupakheti, M., Sciare, J., Müller, T., Wiedensohler, A., Hansen, A.D.A., 2015. The "dual-spot" Aethalometer: an improved measurement of aerosol black carbon with real-time loading compensation. *Atmospheric Measurement Techniques* 8 (5), 1965–1979. <https://doi.org/10.5194/amt-8-1965-2015>.
- Duan, J., Huang, R.J., Lin, C., Dai, W., Wang, M., Gu, Y., Zhong, H., Zheng, Y., Ni, H., Dusek, U., Chen, Y., Li, Y., Chen, Q., Worsnop, D.R., O'Dowd, C.D., Cao, J., 2019. Distinctions in source regions and formation mechanisms of secondary aerosol in Beijing from summer to winter. *Atmos. Chem. Phys.* 19 (15), 10319–10334. <https://doi.org/10.5194/acp-19-10319-2019>.
- Dumka, U.C., Kaskaoutis, D.G., Tiwari, S., Safai, P.D., Attri, S.D., Soni, V.K., Singh, N., Mihalopoulos, N., 2018. Assessment of biomass burning and fossil fuel contribution to black carbon concentrations in Delhi during winter. *Atmos. Environ.* 194, 93–109. <https://doi.org/10.1016/j.atmosenv.2018.09.033>.
- <http://delhiplanning.nic.in/sites/default/files/Highlights%20English%20of%20Economic%20Survey%20of%20Delhi%202018-19.pdf>, 2019–. (Accessed 5 July 2021).
- Fleming, Z.L., Monks, P.S., Manning, A.J., 2012. Review: untangling the influence of air-mass history in interpreting observed atmospheric composition. *Atmos. Res.* 104–105, 1–39. <https://doi.org/10.1016/j.atmosres.2011.09.009>. Elsevier.
- Fröhlich, R., Crenn, V., Setyan, A., Belis, C.A., Canonaco, F., Favez, O., Riffault, V., Slowik, J.G., Aas, W., Aijälä, M., Alastuey, A., Artíñano, B., Bonnaire, N., Bozzetti, C., Bressi, M., Carbone, C., Coz, E., Croteau, P.L., Cubison, M.J., et al., 2015. ACTRIS ACSM intercomparison - Part 2: intercomparison of ME-2 organic source apportionment results from 15 individual, co-located aerosol mass spectrometers. *Atmospheric Measurement Techniques* 8 (6), 2555–2576. <https://doi.org/10.5194/amt-8-2555-2015>.
- ftp, <ftp://arlftp.arlhq.noaa.gov/pub/archives/gdas1>. (n.d.). Index of/pub/archives/gdas1. Retrieved from July 31, 2020, <ftp://arlftp.arlhq.noaa.gov/pub/archives/gdas1>.
- Ganguly, D., Gadhavi, H., Jayaraman, A., Rajesh, T.A., Misra, A., 2005. Single scattering albedo of aerosols over the central India: implications for the regional aerosol radiative forcing. *Geophys. Res. Lett.* 32 (18), 1–4. <https://doi.org/10.1029/2005GL023903>.
- Gani, S., Bhandari, S., Seraj, S., Wang, D.S., Patel, K., Soni, P., Arub, Z., Habib, G., Hildebrandt Ruiz, L., Apte, J., 2018. Submicron aerosol composition in the world's most polluted megacity: the Delhi Aerosol Supersite campaign. *Atmos. Chem. Phys. Discuss.* 5, 1–33. <https://doi.org/10.5194/acp-2018-1066>.
- Gani, S., Bhandari, S., Seraj, S., Wang, D.S., Patel, K., Soni, P., Arub, Z., Habib, G., Hildebrandt Ruiz, L., Apte, J.S., 2019. Submicron aerosol composition in the world's most polluted megacity: the Delhi Aerosol Supersite study. *Atmos. Chem. Phys.* 19 (10), 6843–6859. <https://doi.org/10.5194/acp-19-6843-2019>.
- Guttikunda, S.K., Calori, G., 2013. A GIS based emissions inventory at 1 km × 1 km spatial resolution for air pollution analysis in Delhi, India. *Atmos. Environ.* 67, 101–111. <https://doi.org/10.1016/j.atmosenv.2012.10.040>.
- Guttikunda, S.K., Jawahar, P., 2014. Atmospheric emissions and pollution from the coal-fired thermal power plants in India. *Atmos. Environ.* 92, 449–460. <https://doi.org/10.1016/j.atmosenv.2014.04.057>.
- Hayes, P.L., Ortega, A.M., Cubison, M.J., Froyd, K.D., Zhao, Y., Cliff, S.S., Hu, W.W., Toohey, D.W., Flynn, J.H., Lefer, B.L., Grossberg, N., Alvarez, S., Rappenglück, B., Taylor, J.W., Allan, J.D., Holloway, J.S., Gilman, J.B., Kuster, W.C., De Gouw, J.A., et al., 2013. Organic aerosol composition and sources in Pasadena, California, during the 2010 CalNex campaign. *J. Geophys. Res. Atmos.* 118 (16), 9233–9257. <https://doi.org/10.1002/jgrd.50530>.
- He Lin, Y., Huang, X.-F., Guo, S., Xue, L., Su, Q., Hu, M., Luan, S.-J., Zhang, Y.-H., 2010. Characterization of high-resolution aerosol mass spectra of primary organic aerosol emissions from Chinese cooking and biomass burning. *Atmos. Chem. Phys.* 10 (23), 11535–11543. <https://doi.org/10.5194/acp-10-11535-2010>.
- Hindiaryati, L., 2007. ★★Gas Phase Sulfur, Chlorine and Potassium Chemistry in Biomass Combustion. doctoral(thesis). Technical University of Denmark.
- Hopke, P.K., 2016. Review of receptor modeling methods for source apportionment. *J. Air Waste Manag. Assoc.* 66 (3), 237–259. <https://doi.org/10.1080/10962247.2016.1140693>.
- Hu, H., Yuan, B., Jimenez, J.L., Tang, Q., Peng, J.F., Hu, W., Shao, M., Wang, M., Zeng, L.M., Wu, Y.S., Gong, Z.H., Huang, X.F., He, L.Y., 2013. Insights on organic aerosol aging and the influence of coal combustion at a regional receptor site of central eastern China. *Atmos. Chem. Phys.* 13 (19), 10095–10112. <https://doi.org/10.5194/acp-13-10095-2013>.
- Hu, W., Campuzano-Jost, P., Day, D.A., Croteau, P., Canagaratna, M.R., Jayne, J.T., Worsnop, D.R., Jimenez, J.L., 2017. Evaluation of the new capture vapourizer for aerosol mass spectrometers (AMS) through laboratory studies of inorganic species. *Atmospheric Measurement Techniques* 10 (8), 2897–2921. <https://doi.org/10.5194/amt-10-2897-2017>.
- Hu, W., Hu, M., Hu, W., Jimenez, J.L., Yuan, B., Chen, W., Wang, M., Wu, Y., Chen, C., Wang, Z., Peng, J., Zeng, L., Shao, M., 2016. Chemical composition, sources, and aging process of submicron aerosols in Beijing: contrast between summer and winter. *J. Geophys. Res.* 121 (4), 1955–1977. <https://doi.org/10.1002/2015JD024020>.
- Huang, R.J., Zhang, Y., Bozzetti, C., Ho, K.F., Cao, J.J., Han, Y., Daellenbach, K.R., Slowik, J.G., Platt, S.M., Canonaco, F., Zotter, P., Wolf, R., Pieber, S.M., Bruns, E.A., Crippa, M., Ciarelli, G., Piazzalunga, A., Schwikowski, M., Abbazade, G., et al., 2015. High secondary aerosol contribution to particulate pollution during haze events in China. *Nature* 514 (7521), 218–222. <https://doi.org/10.1038/nature13774>.
- 2013 IPCC, 2013. In: Stocker, T.F., Qin, D., Plattner, G.-K., Tignor, M., Allen, S.25K. (Eds.), IPCC, Climate Change 2013: the Physical Science Basis. Contribution of Working Group I to the Fifth Assessment Report of the Intergovernmental Panel on Climate Change. Boschun.
- IQAir, 2019. World Air Quality Report. In *2019 World Air Quality Report*. <https://www.iqair.com/world-most-polluted-cities/world-air-quality-report-2019-en.pdf>.
- Jain, S., Sharma, S.K., Mandal, T.K., Saxena, M., 2018. Source apportionment of PM₁₀ in Delhi, India using PCA/APCS, UNMIX and PMF. *Particuology* 37, 107–118. <https://doi.org/10.1016/j.partic.2017.05.009>.
- Jaiprakash, 2017. Chemical characterization of PM_{1.0} aerosol in Delhi and source apportionment using positive matrix factorization. *Environ. Sci. Pollut. Control Ser.* 24 (1), 445–462. <https://doi.org/10.1007/s11356-016-7708-8>.
- Jeong, C.-H., Wang, J.M., Evans, G.J., 2016. Source apportionment of urban particulate matter using hourly resolved trace metals, organics, and inorganic aerosol components. *April Atmos. Chem. Phys. Discuss.* 1–32. <https://doi.org/10.5194/acp-2016-189>.
- Khare, P., Baruah, B.P., 2010. Elemental characterization and source identification of PM_{2.5} using multivariate analysis at the suburban site of North-East India. *Atmos. Res.* 95 (1), 148–162. <https://doi.org/10.1016/j.atmosres.2010.07.001>.
- Lalchandani, V., Kumar, V., Tobler, A., M Thamban, N., Mishra, S., Slowik, J.G., Bhattu, D., Rai, P., Satish, R., Ganguly, D., Tiwari, S., Rastogi, N., Tiwari, S., Močnik, G., Prévôt, A.S.H., Tripathi, S.N., 2021. Real-time characterization and source apportionment of fine particulate matter in the Delhi megacity area during late winter. *Sci. Total Environ.* 770, 145324. <https://doi.org/10.1016/j.scitotenv.2021.145324>.
- Lanz, V.A., Alfarra, M.R., Baltensperger, U., Buchmann, B., Hueglin, C., Prévôt, A.S.H., 2007. Source apportionment of submicron organic aerosols at an urban site by factor analytical modelling of aerosol mass spectra. *Atmos. Chem. Phys.* 7 (6), 1503–1522. <https://doi.org/10.5194/acp-7-1503-2007>.
- Li, Q., Cheng, H., Zhou, T., Lin, C., Guo, S., 2012. The estimated atmospheric lead emissions in China, 1990–2009. *Atmos. Environ.* 60, 1–8. <https://doi.org/10.1016/j.atmosenv.2012.06.025>.
- Li, R., Wang, Q., He, X., Zhu, S., Zhang, K., Duan, Y., Fu, Q., Qiao, L., Wang, Y., Huang, L., Li, L., Yu, J.Z., 2020. Source apportionment of PM_{2.5} in Shanghai based on hourly molecular organic markers and other source tracers. *Atmos. Chem. Phys.* 1–26. <https://doi.org/10.5194/acp-2019-951>.
- Lin, Y.C., Hsu, S.C., Lin, C.Y., Lin, S.H., Huang, Y.T., Chang, Y., Zhang, Y.L., 2018. Enhancements of airborne particulate arsenic over the subtropical free troposphere: impact of southern Asian biomass burning. *Atmos. Chem. Phys.* 18 (19), 13865–13879. <https://doi.org/10.5194/acp-18-13865-2018>.
- Liu, S.H., Yan, N.Q., Liu, Z.R., Qu, Z., Wang, H.P., Chang, S.G., Miller, C., 2007. Using bromine gas to enhance mercury removal from flue gas of coal-fired power plants. *Environ. Sci. Technol.* 41 (4), 1405–1412. <https://doi.org/10.1021/es061705p>.
- Manchanda, C., Kumar, M., Singh, V., Faisal, M., Hazarika, N., Shukla, A., Lalchandani, V., Goel, V., Thamban, N., Ganguly, D., Tripathi, S.N., 2021. Variation in chemical composition and sources of PM_{2.5} during the COVID-19 lockdown in Delhi. *Environ. Int.* 153, 106541. <https://doi.org/10.1016/j.envint.2021.106541>.
- Middlebrook, A.M., Bahreini, R., Jimenez, J.L., Canagaratna, M.R., 2012. Evaluation of composition-dependent collection efficiencies for the aerodyne aerosol mass spectrometer using field data. *Aerosol. Sci. Technol.* 46 (3), 258–271. <https://doi.org/10.1080/02786826.2011.620041>.
- Mohr, C., DeCarlo, P.F., Heringa, M.F., Chirico, R., Slowik, J.G., Richter, R., Reche, C., Alastuey, A., Querol, X., Seco, R., Peñuelas, J., Jiménez, J.L., Crippa, M., Zimmermann, R., Baltensperger, U., Prévôt, A.S.H., 2012. Identification and quantification of organic aerosol from cooking and other sources in Barcelona using aerosol mass spectrometer data. *Atmos. Chem. Phys.* 12 (4), 1649–1665. <https://doi.org/10.5194/acp-12-1649-2012>.
- Molina, L.T., Gallardo, L., Andrade, M., Baumgardner, D., Borbor-Córdova, M., Borquez, R., Casassa, G., Cereceda-Balic, F., Dawidowski, L., Garreaud, R., Huneus, N., Lambert, F., McCarty, J.L., McPhee, J., Mena-Carrasco, M., Raga, G.B., Schmitt, C., Schwarz, J.P., 2015. Pollution and its impacts on the south American cryosphere. *Earth's Future* 3 (12), 345–369. <https://doi.org/10.1002/2015EF000311>.
- Nagar, P.K., Singh, D., Sharma, M., Kumar, A., Aneja, V.P., George, M.P., Agarwal, N., Shukla, S.P., 2017. Characterization of PM_{2.5} in Delhi: role and impact of secondary aerosol, burning of biomass, and municipal solid waste and crustal matter. *Environ. Sci. Pollut. Control Ser.* 24 (32), 25179–25189. <https://doi.org/10.1007/s11356-017-0171-3>.
- Nalbandian, H., 2012. In: Trace Element Emissions from Coal. Profiles.
- Ng, N.L., Canagaratna, M.R., Zhang, Q., Jimenez, J.L., Tian, J., Ulbrich, I.M., Kroll, J.H., Docherty, K.S., Chhabra, P.S., Bahreini, R., Murphy, S.M., Seinfeld, J.H.,

- Hildebrandt, L., Donahue, N.M., Decarlo, P.F., Lanz, V.A., Prévôt, A.S.H., Dinar, E., Rudich, Y., Worsnop, D.R., 2010. Organic aerosol components observed in northern hemispheric datasets from aerosol mass spectrometry. *Atmos. Chem. Phys.* 10 (10), 4625–4641. <https://doi.org/10.5194/acp-10-4625-2010>.
- Paatero, P., Eberly, S., Brown, S.G., Norris, G.A., 2014. Methods for estimating uncertainty in factor analytic solutions. *Atmospheric Measurement Techniques* 7 (3), 781–797. <https://doi.org/10.5194/amt-7-781-2014>.
- Paatero, Pentti, Hopke, P.K., 2009. Rotational tools for factor analytic models. *J. Chemometr.* 23 (2), 91–100. <https://doi.org/10.1002/cem.1197>.
- Paatero, Pentti, Hopke, P.K., 2003. Discarding or downweighting high-noise variables in factor analytic models. *Anal. Chim. Acta* 490 (1–2), 277–289. [https://doi.org/10.1016/S0003-2670\(02\)01643-4](https://doi.org/10.1016/S0003-2670(02)01643-4).
- Paatero, Pentti, Tapper, U., 1994. Positive matrix factorization: a non-negative factor model with optimal utilization of error estimates of data values. *Environmetrics* 5 (2), 111–126. <https://doi.org/10.1002/env.3170050203>.
- Pant, P., Harrison, R.M., 2012. Critical review of receptor modelling for particulate matter: a case study of India. *Atmos. Environ.* 49, 1–12. <https://doi.org/10.1016/j.atmosenv.2011.11.060>.
- Pant, P., Shukla, A., Kohl, S.D., Chow, J.C., Watson, J.G., Harrison, R.M., 2015. Characterization of ambient PM_{2.5} at a pollution hotspot in New Delhi, India and inference of sources. *Atmos. Environ.* 109, 178–189. <https://doi.org/10.1016/j.atmosenv.2015.02.074>.
- Petit, J.E., Favez, O., Albinet, A., Canonaco, F., 2017. A user-friendly tool for comprehensive evaluation of the geographical origins of atmospheric pollution: wind and trajectory analyses. *Environ. Model. Software* 88, 183–187. <https://doi.org/10.1016/j.envsoft.2016.11.022>.
- Pope, C.A., Dockery, D.W., 2006. Health effects of fine particulate air pollution: lines that connect. *J. Air Waste Manag. Assoc.* 56 (6), 709–742. <https://doi.org/10.1080/10473289.2006.10464485>.
- Rai, P., Furger, M., El Haddad, I., Kumar, V., Wang, L., Singh, A., Dixit, K., Bhattu, D., Petit, J.-E., Ganguly, D., Rastogi, N., Baltensperger, U., Tripathi, S.N., Slowik, J.G., Prévôt, A.S.H., 2020b. Real-time measurement and source apportionment of elements in Delhi's atmosphere. *Sci. Total Environ.* 742, 140332. <https://doi.org/10.1016/j.scitotenv.2020.140332>.
- Rai, P., Furger, M., Slowik, J.G., Canonaco, F., Fröhlich, R., Hüglin, C., Minguillón, M.C., Petterson, K., Baltensperger, U., Prévôt, A.S.H., 2020a. Source apportionment of highly time-resolved elements during a firework episode from a rural freeway site in Switzerland. *Atmos. Chem. Phys.* 20 (3), 1657–1674. <https://doi.org/10.5194/acp-20-1657-2020>.
- Rupakheti, D., Adhikary, B., Praveen, P.S., Rupakheti, M., Kang, S., Mahata, K.S., Naja, M., Zhang, Q., Panday, A.K., Lawrence, M.G., 2017. Pre-monsoon air quality over Lumbini, a world heritage site along the Himalayan foothills. *Atmos. Chem. Phys.* 17 (18), 11041–11063. <https://doi.org/10.5194/acp-17-11041-2017>.
- Sahu, R., Dixit, K.K., Mishra, S., Kumar, P., Shukla, A.K., Sutar, R., Tiwari, S., Tripathi, S.N., 2020. Validation of low-cost sensors in measuring real-time PM₁₀ concentrations at two sites in Delhi national capital region. *Sensors* 20 (5). <https://doi.org/10.3390/s20051347>.
- Sandradewi, J., Prévôt, A.S.H., Szidat, S., Perron, N., Alfarra, M.R., Lanz, V.A., Weingartner, E., Baltensperger, U.R.S., 2008. Using aerosol light absorption measurements for the quantitative determination of wood burning and traffic emission contribution to particulate matter. *Environ. Sci. Technol.* 42 (9), 3316–3323. <https://doi.org/10.1021/es702253m>.
- Sharma, S.K., Mandal, T.K., Jain, S., Saraswati Sharma, A., Saxena, M., 2016. Source apportionment of PM_{2.5} in Delhi, India using PMF model. *Bull. Environ. Contam. Toxicol.* 97 (2), 286–293. <https://doi.org/10.1007/s00128-016-1836-1>.
- Simoneit, B.R.T., Schauer, J.J., Nolte, C.G., Oros, D.R., Elias, V.O., Fraser, M.P., Rogge, W.F., Cass, G.R., 1999. Levoglucosan, a tracer for cellulose in biomass burning and atmospheric particles. *Atmos. Environ.* 33 (2), 173–182. [https://doi.org/10.1016/S1352-2310\(98\)00145-9](https://doi.org/10.1016/S1352-2310(98)00145-9).
- Stefenelli, G., Pospisilova, V., Lopez-Hilfiker, F.D., Daellenbach, K.R., Hüglin, C., Tong, Y., Baltensperger, U., Prévôt, A.S.H., Slowik, J.G., 2019. Organic aerosol source apportionment in Zurich using an extractive electrospray ionization time-of-flight mass spectrometer (EESI-TOF-MS) – Part 1: biogenic influences and day–night chemistry in summer. *Atmos. Chem. Phys.* 19 (23), 14825–14848. <https://doi.org/10.5194/acp-19-14825-2019>.
- Sueper, D., 2018. Sueper, 2018.
- Sun, J., Shen, Z., Zhang, L., Lei, Y., Gong, X., Zhang, Q., Zhang, T., Xu, H., Cui, S., Wang, Q., Cao, J., Tao, J., Zhang, N., Zhang, R., 2019. Chemical source profiles of urban fugitive dust PM_{2.5} samples from 21 cities across China. *Sci. Total Environ.* 649, 1045–1053. <https://doi.org/10.1016/j.scitotenv.2018.08.374>.
- Sun, Y., Du, W., Fu, P., Wang, Q., Li, J., Ge, X., Zhang, Q., Zhu, C., Ren, L., Xu, W., Zhao, J., Han, T., Worsnop, D.R., Wang, Z., 2016a. Primary and secondary aerosols in Beijing in winter: sources, variations and processes. *Atmos. Chem. Phys.* 16 (13), 8309–8329. <https://doi.org/10.5194/acp-16-8309-2016>.
- Sun, Y., Du, W., Fu, P., Wang, Q., Li, J., Ge, X., Zhang, Q., Zhu, C., Ren, L., Xu, W., Zhao, J., Han, T., Worsnop, D.R., Wang, Z., 2016b. Primary and secondary aerosols in Beijing in winter: sources, variations and processes. *Atmos. Chem. Phys.* 16 (13), 8309–8329. <https://doi.org/10.5194/acp-16-8309-2016>.
- Suvarapu, L.N., Baek, S.O., 2016. Determination of heavy metals in the ambient atmosphere: a review. *Toxicol. Ind. Health* 33 (1), 79–96. <https://doi.org/10.1177/0748233716654827>.
- Tobler, A., Bhattu, D., Canonaco, F., Lalchandani, V., Shukla, A., Thamban, N.M., Mishra, S., Srivastava, A.K., Bisht, D.S., Tiwari, S., Singh, S., Močnik, G., Baltensperger, U., Tripathi, S.N., Slowik, J.G., Prévôt, A.S.H., 2020. Chemical characterization of PM_{2.5} and source apportionment of organic aerosol in New Delhi, India. *Sci. Total Environ.* 745, 140924. <https://doi.org/10.1016/j.scitotenv.2020.140924>.
- Tremper, A.H., Font, A., Priestman, M., Hamad, S.H., Chung, T.C., Pribadi, A., Brown, R. J.C., Goddard, S.L., Grassineau, N., Petterson, K., Kelly, F.J., Green, D.C., 2018. Field and laboratory evaluation of a high time resolution x-ray fluorescence instrument for determining the elemental composition of ambient aerosols. *Atmospheric Measurement Techniques* 11 (6), 3541–3557. <https://doi.org/10.5194/amt-11-3541-2018>.
- Ulbrich, I.M., Canagaratna, M.R., Zhang, Q., Worsnop, D.R., Jimenez, J.L., 2009. Interpretation of organic components from Positive Matrix Factorization of aerosol mass spectrometric data. *Atmos. Chem. Phys.* 9 (9), 2891–2918. <https://doi.org/10.5194/acp-9-2891-2009>.
- Visser, S., Slowik, J.G., Furger, M., Zotter, P., Bukowiecki, N., Canonaco, F., Flechsig, U., Appel, K., Green, D.C., Tremper, A.H., Young, D.E., Williams, P.I., Allan, J.D., Coe, H., Williams, L.R., Mohr, C., Xu, L., Ng, N.L., Nemitz, E., et al., 2015. Advanced source apportionment of size-resolved trace elements at multiple sites in London during winter. *Atmos. Chem. Phys.* 15 (19), 11291–11309. <https://doi.org/10.5194/acp-15-11291-2015>.
- Wang, L., Slowik, J., Tripathi, N., Bhattu, D., Rai, P., Kumar, V., Vats, P., Satish, R., Baltensperger, U., Ganguly, D., Rastogi, N., Sahu, L., Tripathi, S., Prévôt, A., 2020. Source characterization of volatile organic compounds measured by PTR-ToF-MS in Delhi, India. *Atmos. Chem. Phys.* 1–27. <https://doi.org/10.5194/acp-2020-11>.
- Wang, Y.C., Huang, R.J., Ni, H.Y., Chen, Y., Wang, Q.Y., Li, G.H., Tie, X.X., Shen, Z.X., Huang, Y., Liu, S.X., Dong, W.M., Xue, P., Fröhlich, R., Canonaco, F., Elser, M., Daellenbach, K.R., Bozzetti, C., El Haddad, I., Prévôt, A.S.H., et al., 2017. Chemical composition, sources and secondary processes of aerosols in Baoji city of north-west China. *Atmos. Environ.* 158, 128–137. <https://doi.org/10.1016/j.atmosenv.2017.03.026>.
- Yu, J., Yan, C., Liu, Y., Li, X., Zhou, T., Zheng, M., 2018. Potassium: a tracer for biomass burning in Beijing? *Aerosol and Air Quality Research* 18 (9), 2447–2459. <https://doi.org/10.4209/aaqr.2017.11.0536>.
- Zhang, Q., Jimenez, J.L., Canagaratna, M.R., Ulbrich, I.M., Ng, N.L., Worsnop, D.R., Sun, Y., 2011. Understanding atmospheric organic aerosols via factor analysis of aerosol mass spectrometry: a review. *Anal. Bioanal. Chem.* 401 (10), 3045–3067. <https://doi.org/10.1007/s00216-011-5355-y>.
- Zotter, P., Herich, H., Gysel, M., El-Haddad, I., Zhang, Y., Močnik, G., Hüglin, C., Baltensperger, U., Szidat, S., Prévôt, A.S.H., 2017. Evaluation of the absorption Ångström exponents for traffic and wood burning in the Aethalometer-based source apportionment using radiocarbon measurements of ambient aerosol. *Atmos. Chem. Phys.* 17 (6), 4229–4249. <https://doi.org/10.5194/acp-17-4229-2017>.